iScience

CellPress

Article

KDM5A Regulates a Translational Program that Controls p53 Protein Expression

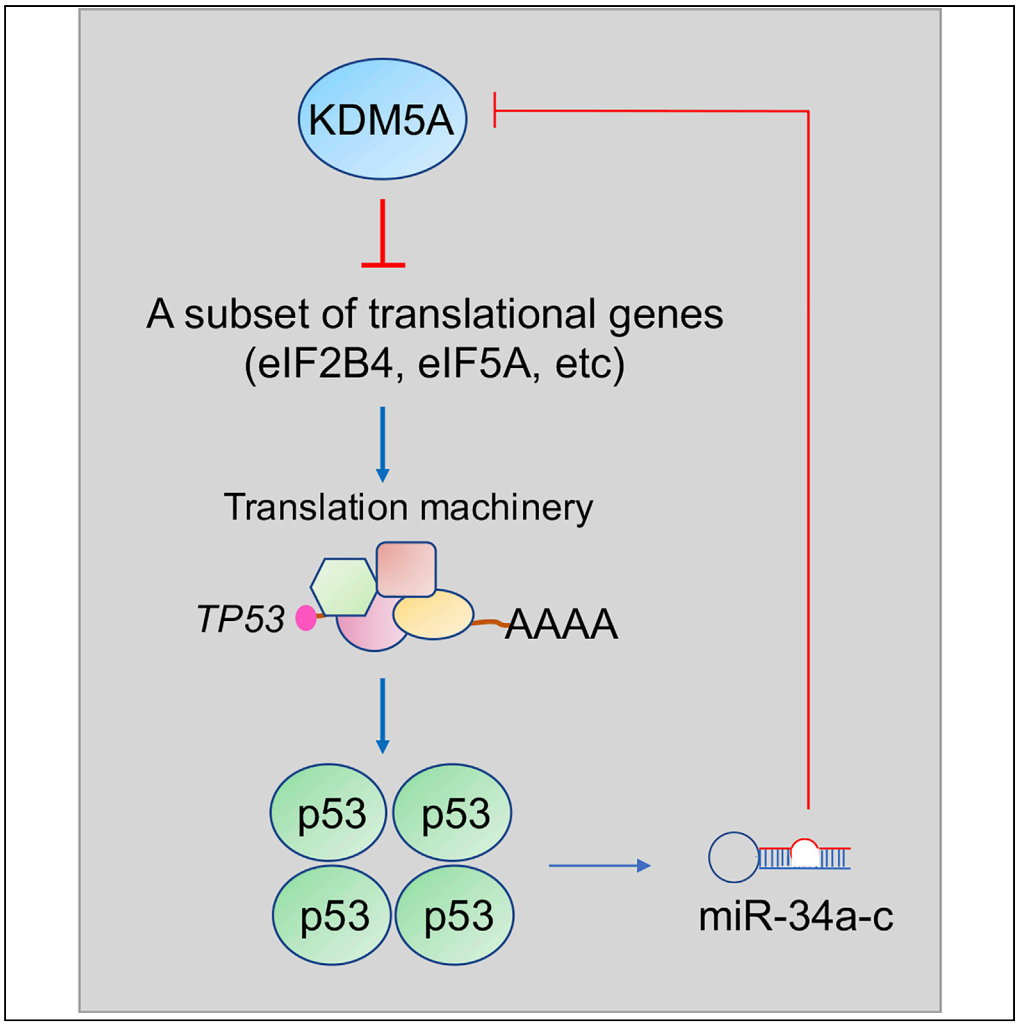

Dongli Hu, Carolyn Jablonowski, Pei-Hsin Cheng, ..., Qin Yan, Andrew M. Davidoff, Jun Yang

jun.yang2@stjude.org

HIGHLIGHTS

Genetic amplification of *KDM5A* tends to be negatively correlated with *TP53* alterations

KDM5A inhibits p53 protein translation by suppressing a subset of translation genes

KDM5A regulates tumor growth in a p53-dependent manner

miR-34 targets KDM5A expression

DATA AND SOFTWARE AVAILABILITY

GSE45967
GSE49854
GSE100511
GSE107221

Hu et al., iScience 9, 84–100
November 30, 2018
https://doi.org/10.1016/j.isci.2018.10.012

iScience

CellPress

Article

KDM5A Regulates a Translational Program that Controls p53 Protein Expression

Dongli Hu,[1,12] Carolyn Jablonowski,[1,12] Pei-Hsin Cheng,[1] Alaa AlTahan,[1] Chunliang Li,[2] Yingdi Wang,[3] Lance Palmer,[4] Cuixia Lan,[5] Bingmei Sun,[6] Ahmed Abu-Zaid,[1] Yiping Fan,[4] Mark Brimble,[1] Nicolas T. Gamboa,[1] Ramhari C. Kumbhar,[7] David Yanishevski,[1] Kyle M. Miller,[7] Guolian Kang,[8] Gerard P. Zambetti,[9] Taosheng Chen,[10] Qin Yan,[11] Andrew M. Davidoff,[1] and Jun Yang[1,13,*]

SUMMARY

The p53 tumor suppressor pathway is frequently inactivated in human cancers. However, there are some cancer types without commonly recognized alterations in p53 signaling. Here we report that histone demethylase KDM5A is involved in the regulation of p53 activity. KDM5A is significantly amplified in multiple types of cancers, an event that tends to be mutually exclusive to p53 mutation. We show that KDM5A acts as a negative regulator of p53 signaling through inhibition of p53 translation via suppression of a subgroup of eukaryotic translation initiation genes. Genetic deletion of KDM5A results in upregulation of p53 in multiple lineages of cancer cells and inhibits tumor growth in a p53-dependent manner. In addition, we have identified a regulatory loop between p53, miR-34, and KDM5A, whereby the induction of miR-34 leads to suppression of KDM5A. Thus, our findings reveal a mechanism by which KDM5A inhibits p53 translation to modulate cancer progression.

INTRODUCTION

The tumor suppressor p53 serves to maintain genomic integrity and regulates the expression of multiple genes that are engaged in cell cycle, apoptosis and metabolism (Lane and Levine, 2010; Vousden and Prives, 2009; Wang and Gu, 2014), as well as immunomodulation (Zitvogel and Kroemer, 2015). It is inactivated in over half of all human cancers via genetic mutations, or MDM2/MDMX- or human papilloma virus (HPV) E6-mediated degradation (Levine and Oren, 2009; Vogelstein and Kinzler, 2004; Vousden and Prives, 2009). Nevertheless, there are some tumor types where these mechanisms of p53 tumor suppressor pathway inactivation do not frequently occur at the time of diagnosis. One such tumor is neuroblastoma (Molenaar et al., 2012; Pugh et al., 2013), the most common pediatric extracranial solid malignancy, responsible for ~15% of cancer deaths in children (Maris, 2010).

Accumulating evidence has implicated epigenetic changes as drivers of cancer (Chi et al., 2010; Dawson and Kouzarides, 2012; Greer and Shi, 2012; Kaelin and McKnight, 2013; Suva et al., 2013; Vogelstein et al., 2013), with many of these being due to alterations in the activity of histone lysine demethylases (KDM) (Dawson and Kouzarides, 2012; Greer and Shi, 2012; Kooistra and Helin, 2012). Several studies indicate that histone demethylases are involved in the regulation of p53 activity. KDM1A has been shown to remove the methyl groups from lysine 370 (K370me2) of the p53 protein directly, thereby suppressing its transcriptional activity (Huang et al., 2007). PHF2 facilitates p53-mediated cell death in response to chemotherapy (Lee et al., 2014), whereas KDM6B can be recruited to p53-bound promoters and enhancer elements with unknown function (Williams et al., 2014). Nevertheless, the roles of other histone demethylases in the regulation of p53 activity have not been well defined. Interestingly, a recent study has shown that methyltransferase SETD8 inhibits the p53 pathway by modulating p53K382me1 levels in high-risk neuroblastoma (Veschi et al., 2017), supporting the hypothesis that additional mechanisms may be involved in the regulation of p53 function in neuroblastoma.

KDM5A (also referred to as RBP2 or JARID1A), an H3K4me3/me2 histone demethylase (Christensen et al., 2007; Klose et al., 2007), is a potential oncogene that is highly expressed in many different cancers (Blair et al., 2011), supports a stem-like phenotype in cancer cells (Sharma et al., 2010), and promotes therapy resistance (Banelli et al., 2015; Hou et al., 2012; Sharma et al., 2010). Genetic ablation of KDM5A hinders tumorigenesis and metastasis (Cao et al., 2014; Lin et al., 2011; Teng et al., 2013). KDM5A is also involved in tumor angiogenesis (Li et al., 2014; Qi et al., 2014). Interestingly, KDM5A can be fused with NUP98 in over

Continued

[1]Department of Surgery, St Jude Children's Research Hospital, 262 Danny Thomas Place, Memphis, TN 38105, USA

[2]Department of Tumor Cell Biology, St Jude Children's Research Hospital, 262 Danny Thomas Place, Memphis, TN 38105, USA

[3]Department of Oncology, St Jude Children's Research Hospital, 262 Danny Thomas Place, Memphis, TN 38105, USA

[4]Department of Computational Biology, St Jude Children's Research Hospital, 262 Danny Thomas Place, Memphis, TN 38105, USA

[5]Department of Clinical Laboratory, Affiliated Qingdao Hiser Hospital of Qingdao University, Qingdao 266033, China

[6]Department of Clinical Laboratory, Qingdao Central Hospital, Affiliated Hospital of Qingdao University, Qingdao 266042, China

[7]Department of Molecular Biosciences, University of Texas at Austin, 100 E 24th St NHB 2.606 Stop A5000, Austin, TX 78712, USA

[8]Department of Biostatistics, St Jude Children's Research Hospital, 262 Danny Thomas Place, Memphis, TN 38105, USA

[9]Department of Pathology, St Jude Children's Research Hospital, 262 Danny Thomas Place, Memphis, TN 38105, USA

[10]Department of Chemical Biology and Therapeutics, St Jude Children's Research Hospital, 262 Danny Thomas

10.5% of pediatric acute megakaryoblastic leukemia (de Rooij et al., 2013; van Zutven et al., 2006). A murine model demonstrated that NUP98/KDM5A is oncogenic in leukemogenesis (Wang et al., 2009). In this study, we examined the effect of all human histone demethylases on p53 activity and found that (1) several KDMs including KDM5A play a role in modulating p53 function; (2) KDM5A is amplified in many types of cancers, an event that tends to be mutually exclusive to p53 gene mutations; (3) KDM5A is overexpressed in high-stage and high-risk neuroblastomas, is associated with a poor outcome, and is negatively correlated with expression of p53 target genes; (4) loss of KDM5A significantly enhances p53 protein accumulation and inhibits tumor growth in wild-type p53, but not mutant p53-expressing colon cancer and neuroblastoma xenograft models; and (5) KDM5A inhibits p53 protein synthesis by suppressing the expression of a subgroup of protein translation genes. We also identified a signaling pathway between KDM5A and miR-34, a p53 target gene that is frequently deleted in high-risk neuroblastomas. Thus, our findings not only support a mechanism by which KDM5A regulates p53 function but also provide a rationale for targeting KDM5A in cancers with wild-type p53.

RESULTS

Identification of Histone Demethylases that Modulate p53 Function

One of the most well-characterized p53 targets is *CDKN1A* (also known as *p21*), which bears two p53 binding sites (5′RE and 3′RE) in the promoter region (Zeng et al., 1997). We therefore used a luciferase reporter carrying the 5′RE and 3′RE of *CDKN1A* to monitor changes in p53 activity that might be affected by altering histone demethylase expression (Figure 1A). We used a focused pooled small interfering RNA (siRNA) library (Yang et al., 2017) (including 32 genes encoding JmjC domain proteins with 17 of them having histone lysine or arginine demethylase activity and 2 genes encoding FAD-dependent demethylases, KDM1A and KDM1B) to demonstrate histone demethylase activity in isogenic $p53^{+/+}$ and $p53^{-/-}$ HCT116 colon cancer cell lines. These isogenic cell lines allowed us to assess the p53-dependent effects only since *CDKN1A* could be activated by other p53-independent epigenetic events such as histone deacetylase (HDAC) inhibition (Gui et al., 2004). We also transfected a Renilla luciferase reporter to serve as an internal control to normalize the *CDKN1A* firefly luciferase. We identified that depletion of *KDM4D*, *KDM5A*, *KDM6B*, *PHF2*, *PHF8*, *C14orf169*, and *JMJD4* resulted in at least a 2-fold greater induction of *CDKN1A* luciferase activity in $p53^{+/+}$ HCT116 cells compared with $p53^{-/-}$ HCT116 cells (Figure 1B). Here we focused on KDM5A for the reasons described below and therefore validated KDM5A-mediated p53 activity. We designed single siRNA oligos and performed RT-PCR. The results showed that depletion of KDM5A led to significant induction of *CDKN1A* in $p53^{+/+}$ HCT116 cells (Figure 1C), consistent with the reporter assay screening.

KDM5A Is Amplified in Several Different Cancers and Is Negatively Correlated with p53 Genetic Mutations

To assess whether any genomic alterations of the KDMs were associated with changes in p53 function, we first examined the genomic amplification or loss of KDMs, since these are important mechanisms by which cancer cells activate proto-oncogenes or inactivate tumor suppressors, using the Tumorscape program, which has high-resolution copy number data amassed from multiple cancer types (all generated through TCGA) (Beroukhim et al., 2010). We found that the *KDM5A* gene was significantly focally amplified across the entire dataset of 10,844 tumors and was located within a focal peak region of the amplicons (q value = 1.91×10^{-33}) (Figure 1D and Table S1). *KDM5A* is significantly focally amplified in 12 of 33 independent cancer types (Table S2). Among these, it is located within a focal peak region of amplification in 11 cancer types (Table S2). Interestingly, after analysis of the tumors from TCGA-PAN cancer data that were well characterized for genetic alterations of *KDM5A*, *MDM2*, and *TP53*, we found that *KDM5A* is significantly associated with genetic mutations of TP53 (Figure 1E). Interestingly, tumors with *KDM5A* amplification tended to be enriched with wild-type p53 when compared with those with *KDM5A* loss (Figures 1E and 1F and Table S3), similar to *MDM2* amplification/loss (Figure 1F). Furthermore, by using the cBioPortal program (Cerami et al., 2012; Gao et al., 2013) we combined five different types of cancer cohorts that had higher incidence of KDM5A amplification (>5%, Figure S1A) for analyses of genetic alteration data of *TP53*, *KDM5A*, *MDM2*, and *CDKN2A* (*P14ARF*) (Figure 1G). p14Arf is a classical tumor suppressor that antagonizes MDM2, thereby playing an important role in regulating p53 protein expression (Kamijo et al., 1998; Stott et al., 1998; Zhang et al., 1998). Among these genetic alterations, despite a tendency of co-occurrence genetic events between *KDM5A* and *MDM2* (Figure 1H), *KDM5A* and *MDM2* amplification tended to be mutually exclusive to *TP53* mutations (Figure 1H). These genetic data suggest that, given the prevalence of its amplification in a variety of human cancers but the negative enrichment with p53 mutations,

Place, Memphis, TN 38105, USA

[11]Department of Pathology, Yale School of Medicine, 310 Cedar St, New Haven, CT 06520, USA

[12]These authors contributed equally

[13]Lead Contact

*Correspondence: jun.yang2@stjude.org

https://doi.org/10.1016/j.isci.2018.10.012

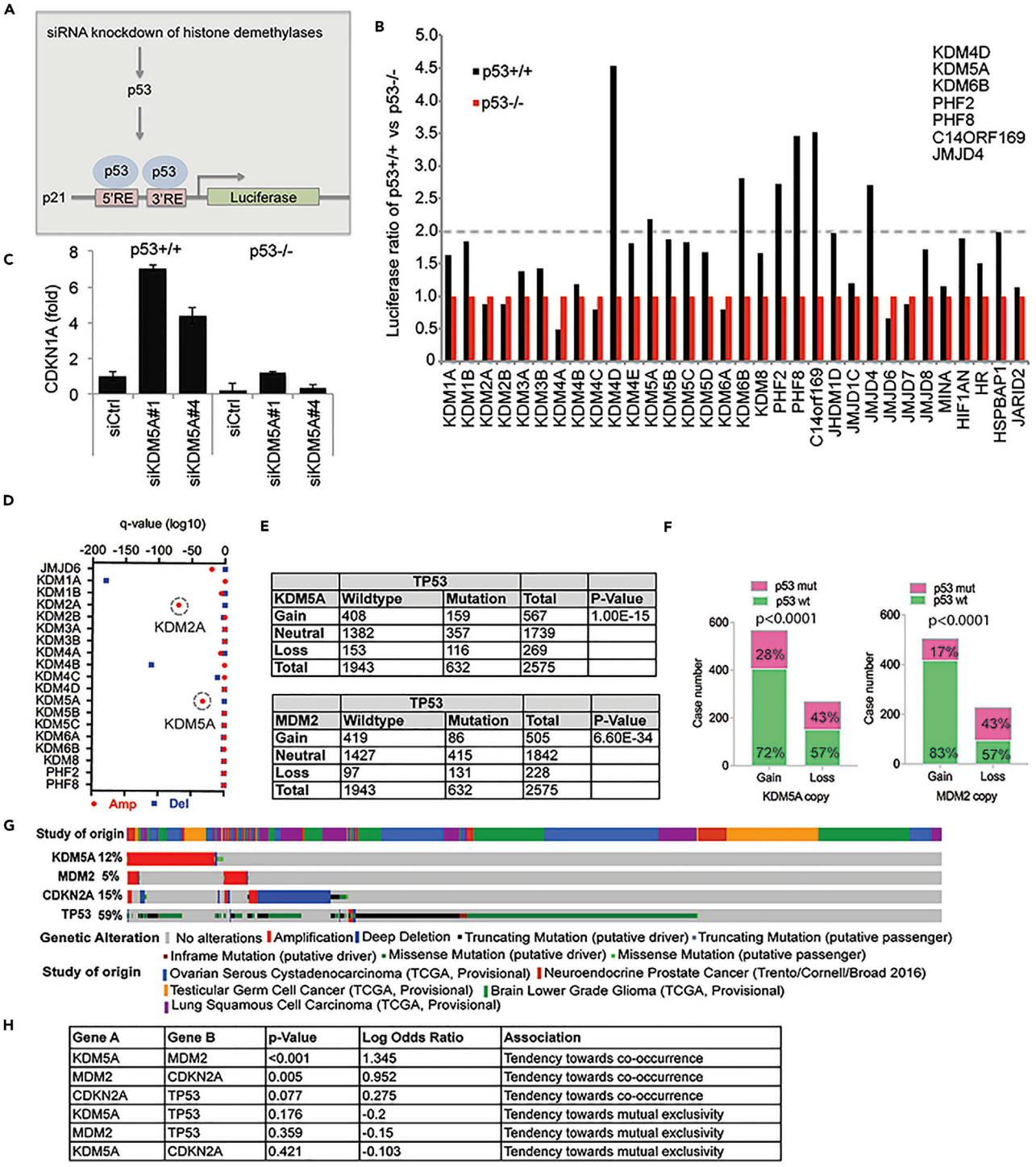

E

	TP53			
KDM5A	Wildtype	Mutation	Total	P-Value
Gain	408	159	567	1.00E-15
Neutral	1382	357	1739	
Loss	153	116	269	
Total	1943	632	2575	

	TP53			
MDM2	Wildtype	Mutation	Total	P-Value
Gain	419	86	505	6.60E-34
Neutral	1427	415	1842	
Loss	97	131	228	
Total	1943	632	2575	

H

Gene A	Gene B	p-Value	Log Odds Ratio	Association
KDM5A	MDM2	<0.001	1.345	Tendency towards co-occurrence
MDM2	CDKN2A	0.005	0.952	Tendency towards co-occurrence
CDKN2A	TP53	0.077	0.275	Tendency towards co-occurrence
KDM5A	TP53	0.176	-0.2	Tendency towards mutual exclusivity
MDM2	TP53	0.359	-0.15	Tendency towards mutual exclusivity
KDM5A	CDKN2A	0.421	-0.103	Tendency towards mutual exclusivity

Figure 1. Identification of Histone Demethylases Engaged in Regulation of p53 Function

(A) Schematic showing the p21 luciferase reporter bearing two p53 binding sites that are subject to modulation by histone demethylases.

(B) Screening results showing the relative luciferase activity that is driven by p53 after siRNA knockdown of the indicated genes.

(C) RT-PCR for *CDKN1A* after 72-hr knockdown of *KDM5A*. Data are mean ± SEM.

(D) Genetic amplification and deletion of histone demethylases across 10,844 cancers. Circled red dots indicate that gene amplification is at its peak. Cutoff q value is 0.25.

Figure 1. *Continued*

(E) Contingency table for the analysis of the distribution frequency of genetic amplification/loss of KDM5A from TCGA PAN-CAN UCSC datasets.

(F) Amplification of *KDM5A* or *MDM2* and *TP53* mutations from TCGA PAN-CAN UCSC data. Chi-square test for statistical analyses, $p < 0.001$.

(G) The genetic alteration of *TP53*, *MDM2*, *KDM5A*, and *CDKN2A* from five cancer cohort data.

(H) The association of genetic alteration of *TP53*, *MDM2*, *KDM5A*, and *CDKN2A* from five cancer cohort datasets.

KDM5A might be a potential proto-oncogene in some types of cancers and may act on the p53 signaling pathway.

KDM5A Overexpression Occurs in High-Stage and High-Risk Neuroblastoma and Is Associated with a Poor Prognosis

The genetic amplification of oncogenes often leads to mRNA overexpression. We assumed that aberrant overexpression of *KDM5A* through mechanisms other than amplification may also be negatively correlated with p53 function. Neuroblastoma, the most common extracranial solid cancer in childhood, rarely bears genetic alterations of p53 (as well as p14Arf or MDM2) at diagnosis (Molenaar et al., 2012; Pugh et al., 2013). We, therefore, speculated that KDM5A might be important in neuroblastoma pathogenesis by suppressing p53 activity. Although amplification of KDM5A does not appear to be a common event in neuroblastoma, overexpression of the *KDM5A* gene was significantly higher in patients with stage 4 disease than in those with other stages, according to the RNA sequencing (RNA-seq) data from a cohort of 498 patients (Su et al., 2014) (Figure 2A). *KDM5A* was also significantly overexpressed in high-risk disease (Figure 2B). In addition, Kaplan-Meier analysis showed that high *KDM5A* expression (median value as a cutoff for *KDM5A* expression levels) was associated with poor outcome in children with neuroblastoma (Figure 2C).

KDM5A Inhibits p53 Signaling

Since KDM5A was highly expressed in high-risk neuroblastomas, we first characterized the function of KDM5A in neuroblastoma, by performing a global gene expression profile analysis after depletion of KDM5A in human neuroblastoma cells. Gene set enrichment analysis (GSEA) showed that depletion of KDM5A in NB-1691 cells (wild-type p53) resulted in induction of the p53 targets (Figure 2D) and negatively correlated with the gene signature upregulated after p53 knockdown (Figure 2E). However, there was no change in the p53 signaling pathways after KDM5A depletion in BE2(C) cells that have mutant p53 (Tweddle et al., 2001). Western blot analysis revealed that p53 and its target p21 were both induced by depletion of KDM5A in NB-1691, SK-N-SH, and IMR32 cells (Figure 2F), three cell lines with wild-type p53. Interestingly, we also observed induction of mutant p53, but not p21, in BE2(C) cells (Figure 2G), suggesting that KDM5A overexpression correlates with reduced p53 expression regardless of its mutation status. We further assessed the correlation of KDM5A and p53 targets. We chose several well-studied p53 target genes including *CDKN1A*, *BBC3* (also named *PUMA*), *BAX*, and *GDF15*, which play important roles in cell-cycle arrest and apoptosis. The results showed that these genes were significantly negatively correlated with *KDM5A* overexpression (Figures 2H and 2I), supporting the hypothesis that KDM5A suppresses p53 function in neuroblastoma. To further assess the role of KDM5A in p53-mediated tumor suppression, we established stable KDM5A depletion using lentiviral small hairpin RNA (shRNA) in NB-1691, SK-N-SH, and BE2(C) cells for xenograft studies. Transduced cells containing the shRNAs were selected for in the presence of 1 μg/mL of puromycin to eliminate the non-transduced cells. KDM5A depletion led to significant tumor growth delay in p53 wild-type cancer cell lines NB-1691 and SK-N-SH (Figures 2J and 2K) but not the p53 mutant BE2(C) cell line (Figure 2L), in accordance with induction of p53 targets before the establishment of xenografts (Figures 2J–2L).

To address whether the above findings represented a general mechanism across different cancer lineages, we included several different types of cancer cell lines bearing wild-type p53 or no p53. First, we performed GSEA after depletion of KDM5A in $p53^{+/+}$ and isogenic $p53^{-/-}$ HCT116 colon cancer cells. Again, this revealed that KDM5A loss resulted in high activity of p53 pathways in $p53^{+/+}$ HCT116 cells (Figures 3A–3C) but not in $p53^{-/-}$ HCT116 cells (Figure S1B). Molecular concept analysis further demonstrated that loss of KDM5A function in $p53^{+/+}$ HCT116 cells led to the expression of genes associated with various p53 signatures, as well as chemotherapy- and ionizing-radiation-induced signatures (Figure 3D). We then assessed protein expression of p53 targets and found that p21, PUMA, TIGAR, and MDM2 were upregulated after KDM5A depletion across several types of cancer cell lines including colon cancer, osteosarcoma, and lung cancer (Figures 3E–3G), in accordance with the induced p53 protein, demonstrating the ability of

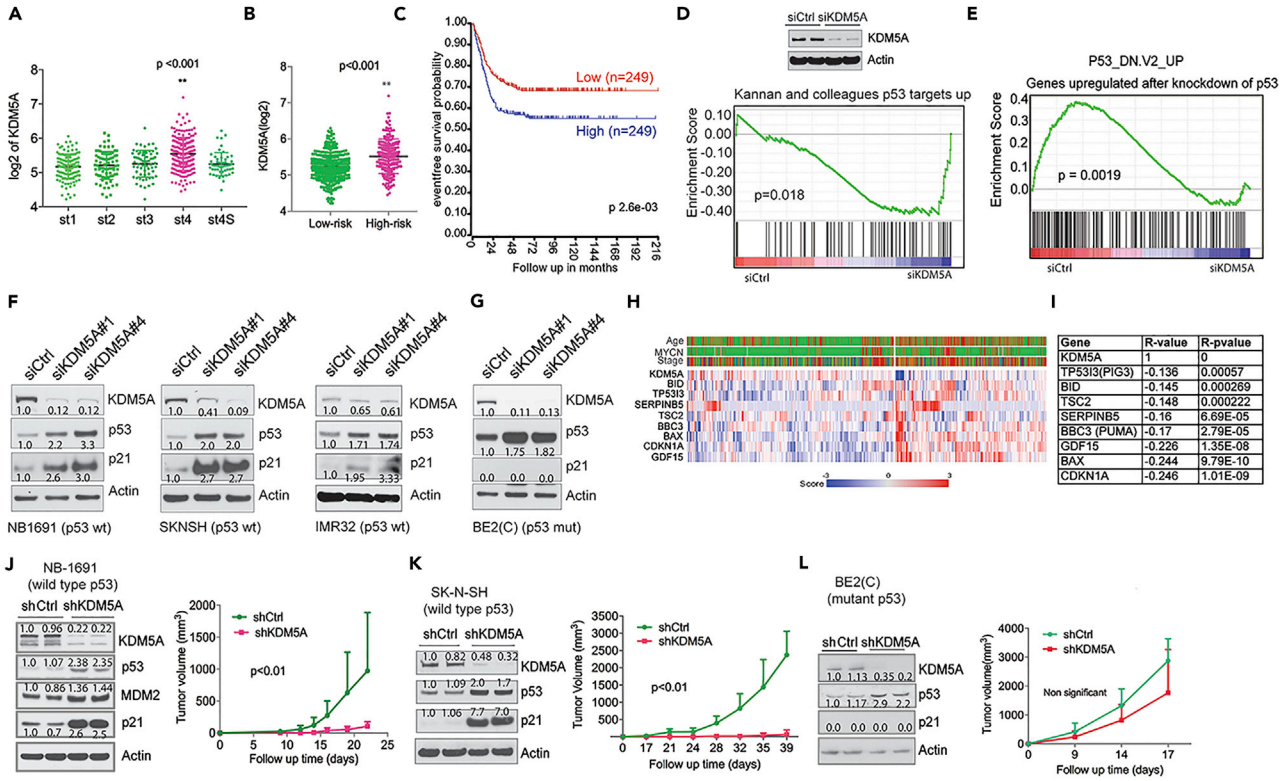

Figure 2. KDM5A Inhibits p53 Function in Neuroblastoma

(A) *KDM5A* expression in different International Neuroblastoma Staging System (INSS) stages of neuroblastoma (Cohort SEQC, GSE62564).

(B) *KDM5A* expression in low- and high-risk neuroblastomas (Cohort SEQC, GSE62564).

(C) Kaplan-Meier analysis of the association of event-free survival with *KDM5A* expression (Cohort SEQC, GSE62564).

(D) GSEA shows that genes upregulated by KDM5A knockdown in NB-1691 cells is associated with a gene set of p53 targets. Western blot analysis of indicated proteins after 72-hr knockdown of KDM5A.

(E) GSEA shows that genes downregulated by KDM5A knockdown in NB-1691 cells is associated with a gene set unregulated by p53 knockdown.

(F and G) Western blot analysis of indicated proteins after 72-hr knockdown of KDM5A in (F) NB1-691, SK-N-SH, and IMR-32 and (G) BE2(C) cells. Band intensity was quantified by ImageJ and normalized to loading control.

(H) Heatmap for gene expression of KDM5A and p53 targets from cohort GSE45547.

(I) Spearman correlation of KDM5A and p53 target genes from cohort GSE45547.

(J–L) Tumor volume curves of (J) NB-1691, (K) SK-N-SH, and (L) BE2(C) neuroblastoma xenografts with lentiviral-mediated shRNA knockdown of KDM5A or control (n = 5 per group). Data are mean ± SEM. Left panel shows western blot analysis of KDM5A knockdown by shRNA before tumor cell implantation. Band intensity was quantified by ImageJ and normalized to loading control. p value was calculated by ANOVA test.

KDM5A to suppress p53 signaling in a wide variety of human cancer cell lines. The induction of p53 by loss of KDM5A was further validated by knocking out KDM5A using CRISPR/Cas9 at two different genomic loci of the *KDM5A* gene from five individual clones that were derived from single cells (Figure S1C). Conversely, overexpression of KDM5A reduced p53 expression, and its target p21 expression (Figure 3H). We further assessed the expression of KDM5A and p53 target genes in a variety of different types of cancer cohorts. The results showed that KDM5A overexpression was negatively correlated with the expression of p53 targets (Figures 3I–3L, and data not shown), suggesting that repression of p53 activity by KDM5A is common across many cancers. Consistent with the tumor suppressive functions of p53, depletion of KDM5A significantly reduced cell colony formation in $p53^{+/+}$ but not $p53^{-/-}$ cancer cells (Figures S1D and S1E). We also generated lentiviral-mediated shRNA knockdown of KDM5A in isogenic $p53^{+/+}$ and $p53^{-/-}$ HCT116 cells (Figure 3M), which allowed us to evaluate the p53 effect more specifically. Again, depletion of KDM5A resulted in significant reduction of tumor growth in the $p53^{+/+}$ but not in the $p53^{-/-}$ xenografts (Figure 3M). Interestingly, after analysis of the expression of KDM5A and p53 in three HCT116 xenografts per group that were randomly chosen, we found that KDM5A re-expressed in all tumor samples of $p53^{+/+}$ HCT116 but not in $p53^{-/-}$ HCT116 and p53 expression was restored back to the same levels as the control (Figure 3N), suggesting that shRNA knockdown of KDM5A confers a selective pressure on p53 wild-type cells, or that it was

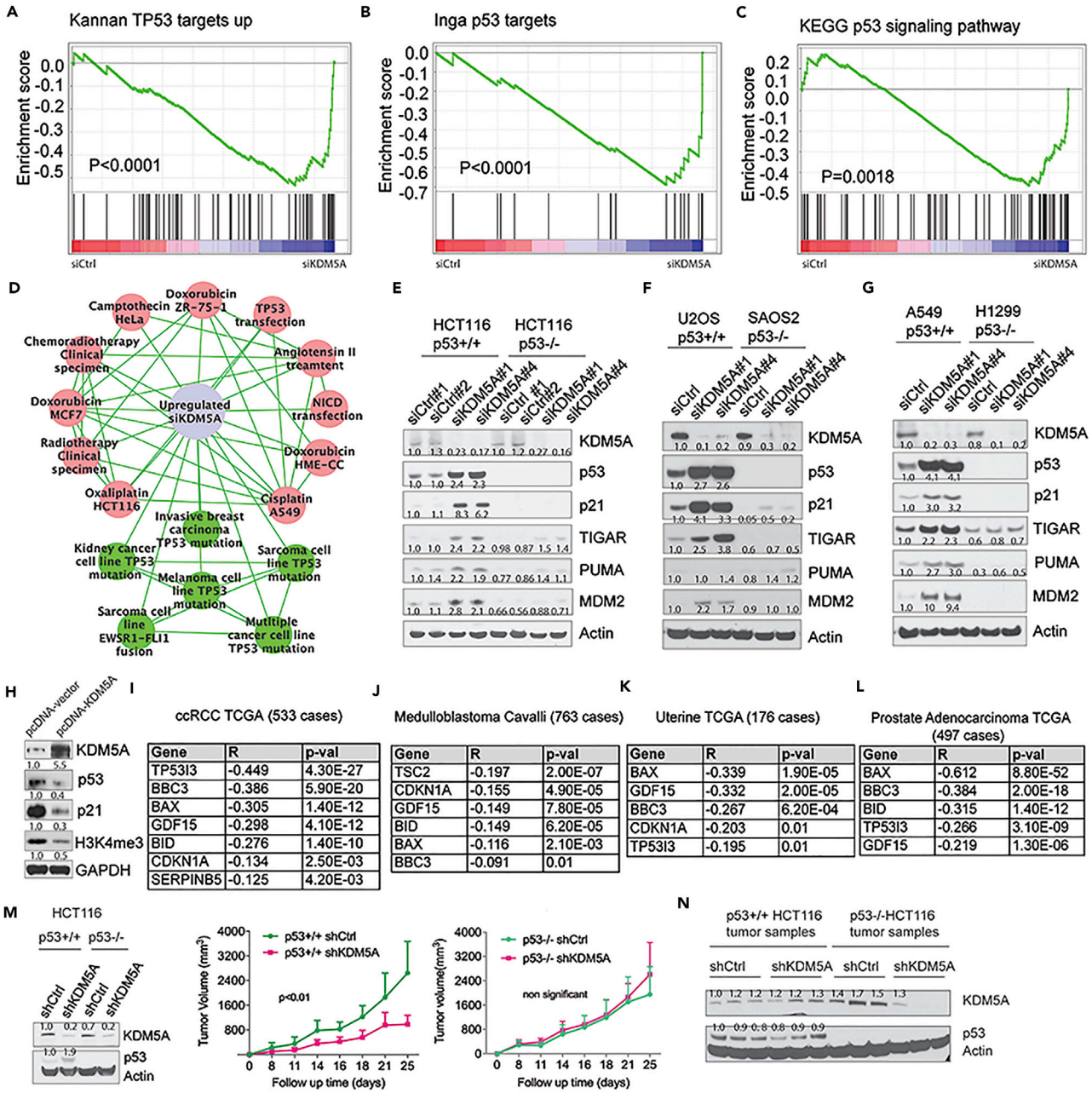

Gene	R	p-val
TP53I3	-0.449	4.30E-27
BBC3	-0.386	5.90E-20
BAX	-0.305	1.40E-12
GDF15	-0.298	4.10E-12
BID	-0.276	1.40E-10
CDKN1A	-0.134	2.50E-03
SERPINB5	-0.125	4.20E-03

Gene	R	p-val
TSC2	-0.197	2.00E-07
CDKN1A	-0.155	4.90E-05
GDF15	-0.149	7.80E-05
BID	-0.149	6.20E-05
BAX	-0.116	2.10E-03
BBC3	-0.091	0.01

Gene	R	p-val
BAX	-0.339	1.90E-05
GDF15	-0.332	2.00E-05
BBC3	-0.267	6.20E-04
CDKN1A	-0.203	0.01
TP53I3	-0.195	0.01

Gene	R	p-val
BAX	-0.612	8.80E-52
BBC3	-0.384	2.00E-18
BID	-0.315	1.40E-12
TP53I3	-0.266	3.10E-09
GDF15	-0.219	1.30E-06

Figure 3. KDM5A Broadly Suppresses p53 Signaling Pathway

(A) GSEA shows that genes upregulated after KDM5A depletion in $p53^{+/+}$ HCT116 cells is associated with a gene set of Kannan TP53 targets up.

(B) GSEA shows that genes upregulated after KDM5A depletion in $p53^{+/+}$ HCT116 cells is associated with a gene set of Inga p53 targets.

(C) GSEA shows that genes upregulated after KDM5A depletion in $p53^{+/+}$ HCT116 cells is associated with a gene set of KEGG p53 signaling pathway.

(D) Molecular concept analysis of genes upregulated after KDM5A depletion in $p53^{+/+}$ HCT116 cells.

(E–G) Western blot analysis with the indicated antibodies after 72-hr KDM5A depletion in (E) HCT116 ($p53^{+/+}$ and $p53^{-/-}$), (F) U2OS and SAOS2, and (G) A549 and H1299 cells. Band intensity was quantified by ImageJ and normalized to loading control.

(H) Effect of KDM5A overexpression in HCT116 cells. Cells transfected with either an empty vector or a plasmid overexpressing KDM5A were subject to western blot analysis. Band intensity was quantified by ImageJ and normalized to loading control.

(I–L) Spearman correlation of KDM5A and p53 target genes from cohort of renal cell carcinoma (I, TCGA ID: KIRC), medulloblastoma (J, GSE85217), uterine cancer (K, TCGA ID: UCEC), and prostate adenocarcinoma (L, TCGA ID: PRAD).

Figure 3. *Continued*

(M) Tumor volume curves of isogenic $p53^{+/+}$ and $p53^{-/-}$ HCT116 xenografts with lentiviral-mediated shRNA knockdown of KDM5A or control (n = 5/group). Data are mean ± SEM. Left panel shows western blot analysis of KDM5A knockdown by shRNA before implantation. p value was calculated by ANOVA test. (N) Western blot analysis of KDM5A and p53 expression in three terminal tumor samples/group in $p53^{+/+}$ and $p53^{-/-}$ HCT116 xenografts. Band intensity was quantified by ImageJ and normalized to loading control.

due to selection of rare clones that were not transduced by KDM5A shRNA. We therefore hypothesize that *KDM5A* may reflect the response of cancer cells to therapies that activate the p53 pathway. Indeed, the data from the Cancer Therapeutics Response Portal (Rees et al., 2016), which links genetic, lineage, and other cellular features of cancer cell lines to small-molecule sensitivity, showed that cancer cells expressing higher *KDM5A* were more sensitive to chemotherapeutic drugs such as etoposide, doxorubicin, and cytarabine (Figure S1F). However, *KDM5B*, a paralog of *KDM5A*, was correlated with drug sensitivity to tyrosine kinase inhibitors and mitogen-activated protein kinase inhibitors (Figure S1G). Taken together, these results demonstrate that KDM5A plays an important role in suppressing p53 function in neuroblastoma and other p53 wild-type-expressing tumors, further suggesting that KDM5A is a regulator of the p53 signaling pathway in most cancers if not all. Therefore, in the following studies, we mainly used the HCT116 colon cancer cell line as the model to dissect the molecular mechanism by which KDM5A regulates p53 expression because this cell line is more easily manipulated genetically and pharmacologically.

KDM5A Inhibits p53 Protein Synthesis

We next sought to understand the mechanism by which KDM5A regulates the p53 signaling pathway in cancer cells. To define the mechanism by which KDM5A suppresses p53 expression, we first tested whether KDM5A directly regulates p53 transcription. Real-time PCR revealed that *TP53* mRNA was modestly decreased, although *CDKN1A* was greatly upregulated by KDM5A depletion in p53 wild-type HCT116 cells (Figure 4A), suggesting that KDM5A regulates p53 expression at a post-transcriptional level. Normally, p53 is a very labile protein that is subject to proteasomal degradation (Kruse and Gu, 2009). In response to cellular stress, such as DNA damage, p53 undergoes post-translational modifications such as phosphorylation at serine 15 and serine 20, which result in the displacement of MDM2 from the N terminus of p53, with consequent stabilization of the p53 protein (Toledo and Wahl, 2006). We found that the DNA-damaging agent doxorubicin induced phosphorylation of p53 Serine 15 but KDM5A depletion did not (Figure 4B), nor did it reduce the protein-protein interaction between MDM2 and p53 (Figure 4C). KDM5A knockdown also did not significantly alter the half-life of p53 when protein synthesis was blocked by cycloheximide (Figure 4D, top panel), whereas treatment of cells with doxorubicin and Nutlin-3, a compound that disrupts the p53-MDM2 interaction, significantly stabilized p53 protein (Figure 4D, bottom panel). These data suggest that KDM5A does not regulate p53 expression through MDM2-mediated degradation. Conversely, when the proteasome inhibitor MG132 was used to block p53 degradation, the amount of newly synthesized p53 protein labeled with S^{35} was much greater after KDM5A depletion, although the total newly synthesized and total protein were not (Figures 4E and S2A), suggesting that KDM5A regulates p53 protein synthesis specifically.

To further validate this, we used alternative approaches to assess the role of KDM5A in the regulation of p53 synthesis. First, we introduced into HCT116 cells a heterologous luciferase reporter in which the p53 coding sequence was replaced by the coding sequence for luciferase, whereas the 5′ and 3′ UTRs of p53 remained intact. The mRNA expression of this reporter was driven by a heterologous promoter, but its translation should be regulated by the same machinery as endogenous p53 because the 5′- and -3′-UTRs of p53 were intact. In these experiments, KDM5A knockdown significantly enhanced the luciferase activity in both $p53^{+/+}$ and $p53^{-/-}$ HCT116 cells (Figure 4F), supporting the hypothesis that KDM5A regulates p53 translation. Next, we tested the effect of two compounds, rocaglamide (Roc A) and cymarin, which specifically inhibit protein translation (Didiot et al., 2013; Rodrigo et al., 2012). We found that when these two compounds were administered, the amount of p53 protein induced by KDM5A depletion was reduced to basal levels, without significantly downregulating p53 mRNA expression (Figures 4G and S2B); however, the p53 protein induced by Nutlin-3 compounds (Nutlin-3b is much less potent than Nutlin-3a), was only partially affected by protein translation inhibitors (Figure 4G). These data indicate that inhibition of protein translation reduced KDM5A-depletion- but not Nutlin-3-induced (via p53 stabilization) enhanced p53 expression. Finally, we found that KDM5A depletion resulted in increased p53 expression in RC10.1 cells (Figure S2C). Rapid degradation of p53 in this cell line normally occurs because these cells, derived from RKO cells, have been engineered to express the HPV E6 oncoprotein (Kessis et al., 1993). However, the increased p53 expression in these cells due to depletion of KDM5A partly overwhelmed the degradation by E6, allowing for the detection of p53. Taken together, these data further support our hypothesis that KDM5A inhibits p53 expression via a mechanism that is involved in p53 protein translation.

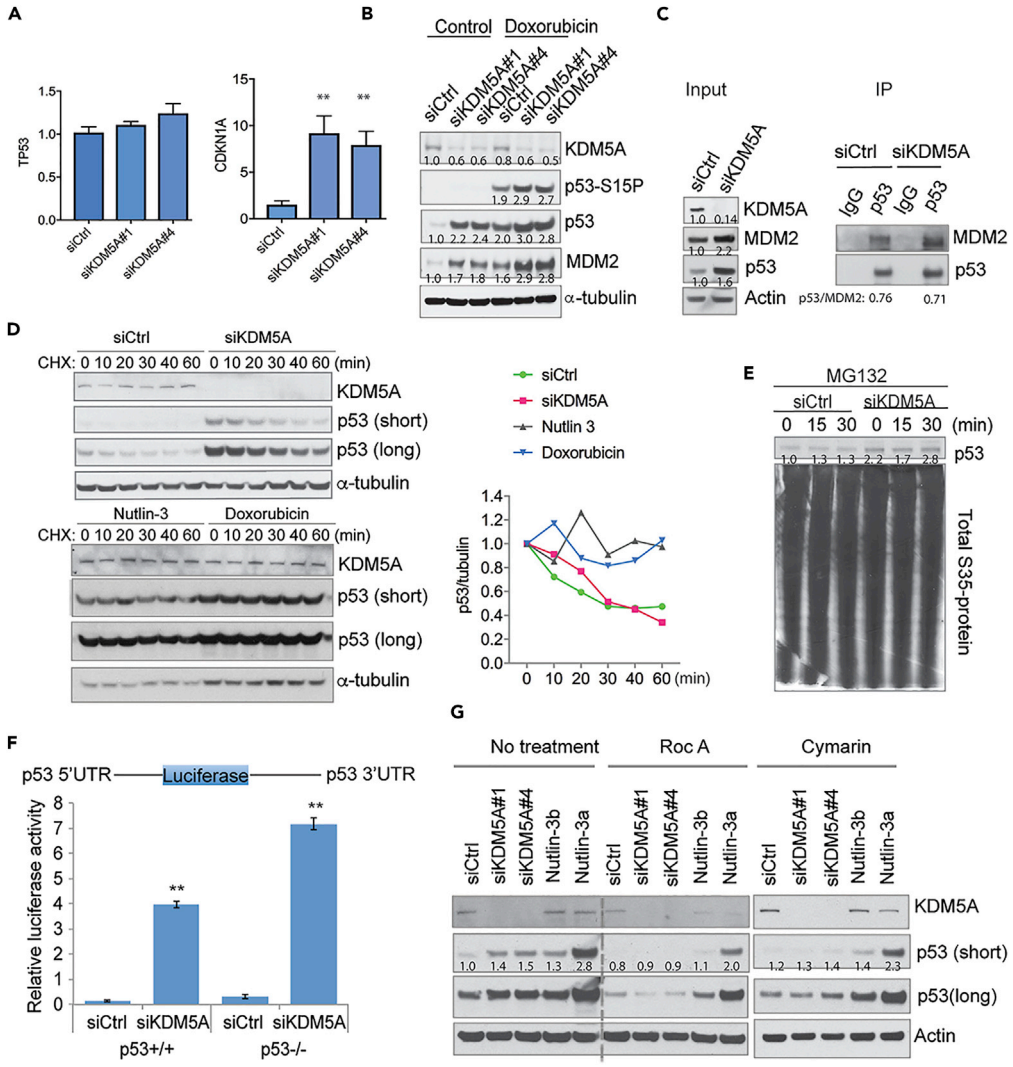

Figure 4. KDM5A Regulates p53 Translation

(A) *TP53* and *CDKN1A* mRNA assessed by RT-PCR after 72-hr knockdown of KDM5A in $p53^{+/+}$HCT116 cells. Data are mean ± SEM. Biological triplicates with technical triplicates for each were performed for Student's t test. **p < 0.01.

(B) Western blot after 48-hr knockdown of KDM5A in A549 cells, followed by 24-hr treatment with 1ug/mL of doxorubicin. Band intensity was quantified by ImageJ and normalized to loading control.

(C) Immunoprecipitation assay for assessment of p53-MDM2 interaction after 72-hr knockdown of KDM5A in $p53^{+/+}$ HCT116 cells. Band intensity was quantified by ImageJ and normalized to loading control.

(D) Assessment of p53 half-life by western blot of protein from HCT116 cells treated with 50 μg/mL of cycloheximide after siRNA knockdown (48 hr) and 5 μM of Nutlin-3 (24 hr) or 0.5 μg/mL of doxorubicin (24hr). ImageJ was used to quantify the western blot bands for the graph on the right.

(E) Pulse-chase results with S^{35} labeling of HCT116 cells in the presence of 5 μM MG132 after 48-hr KDM5A knockdown. p53 band intensity was quantified by ImageJ and normalized to total proteins.

(F) A luciferase reporter assay demonstrating the effect of KDM5A on heterologous expression from a cassette bearing intact 5′UTR and -3′UTR of p53. After 24 hr siRNA knockdown of KDM5A in $p53^{+/+}$ and $p53^{-/-}$ HCT116 cells by reverse transfection, 2.4 μg of p53-UTR firefly luciferase reporter plasmid and 0.1 μg pRL *Renilla* Luciferase Control Reporter Vector were transfected. After 48 hr, cells were harvested for the dual luciferase assay. Data are mean ± SEM. Biological triplicates with technical triplicates for each were performed for Student's t test. **p < 0.01.

(G) After 48-hr knockdown of KDM5A or Nutlin-3 treatment, HCT116 cells were treated with 100 nM of rocaglamide (Roc A) and 100 nM of cymarin for 24 hr. Western blot was used for assessment of p53 expression. Intensity of p53 bands with short exposure were quantified by ImageJ and normalized to loading control.

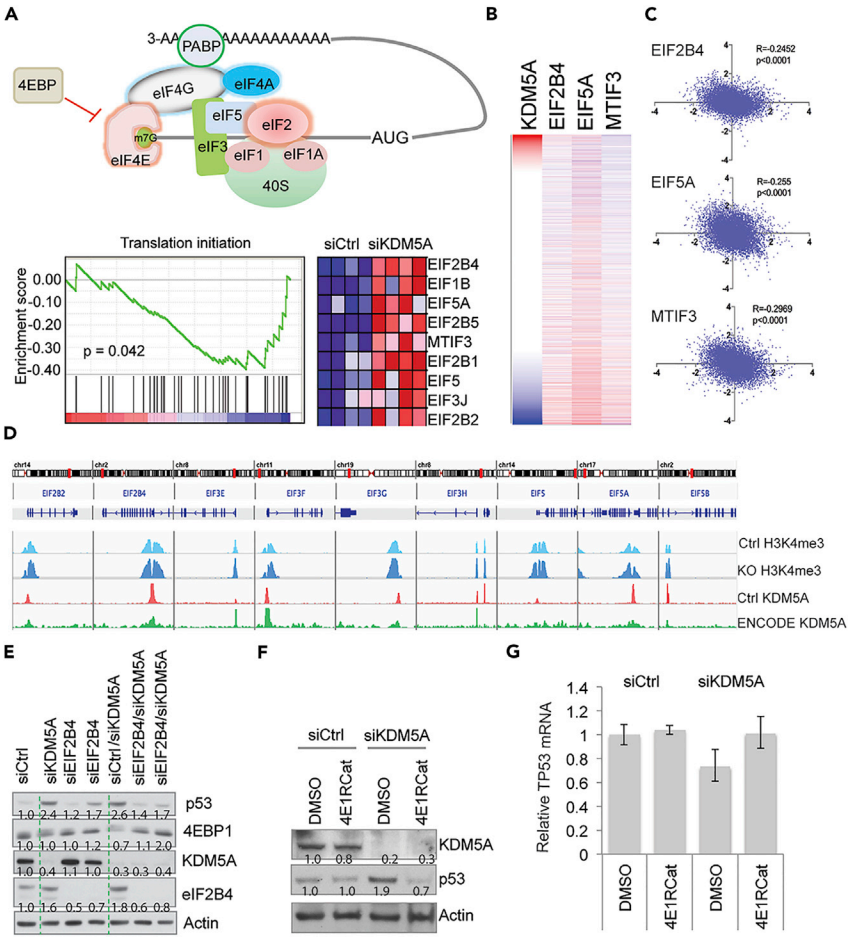

Figure 5. KDM5A Regulates p53 Expression by Modulating Translation Initiation

(A) Schematic showing the protein complexes involved in translation initiation. GSEA shows that the translation initiation pathway is upregulated by KDM5A depletion in isogenic $p53^{+/+}$ and $p53^{-/-}$ HCT116 cells.

(B) Heatmap for gene expression of *KDM5A*, *EIF2B4*, *EIF5*, and *MTIF3* from TCGA PAN-CAN data analyzed by UCSC Xena program.

(C) Spearman correlation of KDM5A and *EIF2B4*, *EIF5A*, and *MTIF3* from PAN-CAN TCGA data.

(D) ChIP-seq data shows KDM5A binding at the genomic loci of translation initiation genes in HCT116 cells (pink) and human embryonic stem cells from ENCODE data (green), and H3K4me3 peaks at the genomic loci of translation initiation genes before (light blue) and after KDM5A disruption by CRISPR/Cas9 (dark blue). Peak scale of 100 for H3K4me3 and KDM5A in HCT116 cells, and 75 for KDM5A ENCODE data.

(E) Western blot assessment of p53 after 72-hr depletion of KDM5A and eIF2B4 in HCT116 cells.

(F) Western blot assessment of p53 expression in HCT116 cells treated with 4E1RCat for 24-hr after KDM5A depletion. Intensity of p53 bands were quantified by ImageJ and normalized to loading control.

(G) RT-PCR assessing the expression of TP53 mRNA from (E). Data are mean ± SEM. Technical triplicates for each were performed.

KDM5A Regulates the Expression of Genes Involved in Translation

Protein translation can be divided into four phases: initiation, elongation, termination, and ribosome recycling (Bhat et al., 2015). We sought to determine at what phase KDM5A was acting. Translation initiation is the most important and complicated step of the translation process and involves many factors and multiple complexes (Figure 5A). Our gene expression profiling analysis revealed that KDM5A depletion resulted in upregulation of a signature containing genes involved in translation initiation but not other steps of translation (Figure 5A), indicating that KDM5A inhibits a subgroup of translation initiation genes. We further analyzed the RNA-seq data from the PAN-CAN dataset and confirmed that expression of *KDM5A* and *EIF2B4*, *EIF5A*, and *MTIF3* were inversely correlated (Figures 5B and 5C), supporting that KDM5A

suppresses the expression of these genes. To explore whether KDM5A was directly involved in the expression of these translation initiation genes, we performed chromatin immunoprecipitation sequencing (ChIP-seq) analysis to determine whether KDM5A bound these genes. Our ChIP-seq data revealed that, among the approximately 5,000 genomic regions bound by KDM5A (Table S4), nearly 100 genes were involved in translation and many of these encoded ribosomal proteins, based on canonical signaling pathway analysis (Table S5). Many of these proteins engage in translation initiation (Figure 5D). We also analyzed the ENCODE ChIP-seq data in which data on KDM5A genomic binding in human embryonic stem cells are available. We found that the genomic loci of these target genes bound by KDM5A were significantly correlated (Figures 5D and S3A), which corroborated our ChIP-seq data.

KDM5A is a histone demethylase that removes H3K4me3/me2. To explore the role of the histone demethylase activity of KDM5A in the regulation of translation initiation genes, we removed KDM5A expression in HCT116 cells using CRISPR/Cas9 and performed ChIP-seq to assess the H3K4me3 changes. The results showed that KDM5A genomic binding sites overlapped with H3K4me3 peaks (Figure 5D and Table S6), and deletion of KDM5A led to an increase in H3K4me3 levels at the promoter regions on these genes (Figure 5D), in line with its histone demethylase activity. Interestingly, we noticed that H3K4me3 was also upregulated at the locus of *TP53* in KDM5A KO cells (Figure S3B), despite the mRNA levels of *TP53* not being altered in these cells (Figure 4A).

To validate whether increased translation initiation was responsible for the upregulation of p53 protein, we studied eIF2B4, the component of the eIF2 complex that regulates the assembly of the 43S pre-initiation complex (PIC) during translation initiation (Bhat et al., 2015). Knockdown of eIF2B4 prevented the induction of p53 associated with depletion of KDM5A (Figure 5E), confirming that KDM5A regulates p53 expression by modulating translation initiation. Interestingly, we also found that downregulation of 4EBP1 due to KDM5A depletion was rescued by co-depletion of eIF2B4 (Figure 5E). 4EBP1 inhibits translation initiation by competing with eIF4E, which forms a complex with eIF4A and eIF4G, called eIF4F, leading to 48S PIC assembly (Bhat et al., 2015). We therefore tested eIF4A2 function and found that loss of eIF4A2 largely rescued the phenotype of p53 induction (Figure S3C). eIF4A2 was able to bind the p53 mRNA (Figure S3D). We further treated cells with 4E1RCat, a compound that interferes with protein translation initiation by preventing the assembly of the eIF4F complex (Cencic et al., 2011). The data showed that 4E1Rcat largely rescued the KDM5A effect on p53 protein accumulation (Figure 5F), but had no effect on *TP53* mRNA expression (Figure 5G). To further analyze the correlation of KDM5A targets with signaling pathways, we used a connectivity map to compare the transcriptome of KDM5A with gene profiles resulting from gene knockdown, gene overexpression, or compound treatment. Despite the upregulation of a subgroup of translation genes (Figure 5A), the top hits highly correlated with KDM5A knockdown-induced transcriptomes were global protein synthesis inhibitors including emetine, verrucarin-a, and homoharringtonine (Table S7). Taken together, these data indicate that KDM5A regulates p53 translation by modulating the expression of protein translation genes.

Enhanced p53 Protein Expression after KDM5A Deletion Is Directly Regulated through Protein Synthesis of *TP53*

Although we had used pulse-chase with S^{35} labeling to show that KDM5A regulates p53 protein synthesis (Figure 4E), we further investigated the mechanism by using two approaches: (1) polysomal profiling to assess whether *TP53* mRNA is more enriched in polysomes (high translation efficiency) than monosomes (low translation efficiency) and (2) Click-iT labeling to assess the newly synthesized p53 protein and total new proteins after KDM5A knockout (Figure 6). The results showed that p53 expression was greatly increased after KDM5A knockout (Figure 6A), consistent with results obtained by siRNA and shRNA of KDM5A. We then used a sucrose gradient (5%–50% of sucrose) method to perform the polysome fractionation (Figure 6B) and extracted total RNA from each fraction (Figure 6C), followed by quantification of the percentage of *TP53* mRNA in each fraction (Figure 6D). Indeed, KDM5A deletion resulted in an enrichment of *TP53* mRNA in the heavy polysome fractions (Figure 6D), suggesting a higher rate of p53 protein synthesis. Importantly, KDM5A knockout had no effect on the total steady-state p53 mRNA levels (Figure 6E).

The Click-iT labeling, a similar approach to S^{35} pulse labeling, uses a methionine analog L-azidohomoalanine (AHA) to label newly synthesized proteins after methionine-free medium starvation (Figure 6F). Then a Click-iT chemistry-based reaction brings the alkyne-modified biotin to the AHA-incorporated polypeptides. The total

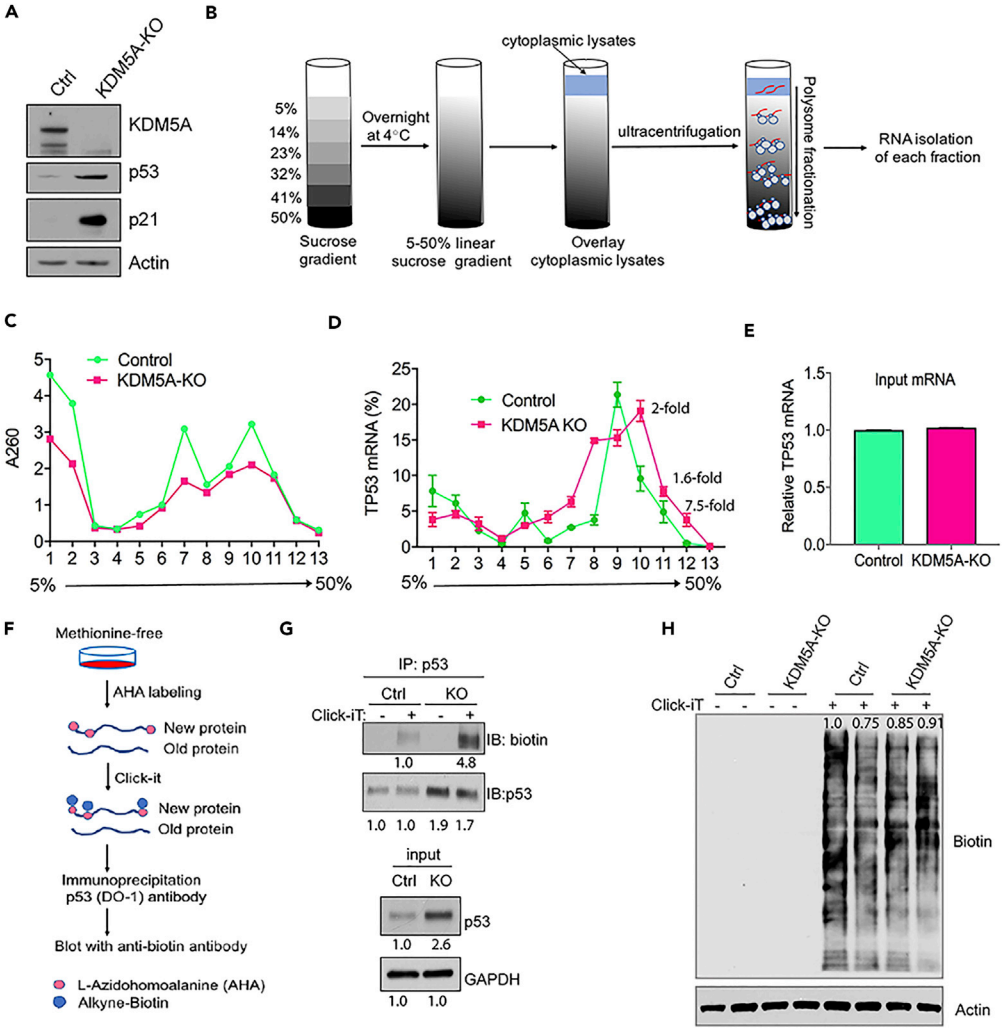

Figure 6. Enhanced p53 Protein Expression after KDM5A Deletion Is Directly Regulated by Protein Synthesis of *TP53*

(A) Western blot analysis of p53 and p21 proteins in KDM5A knockout HCT116 cells compared with HCT116 control cells.

(B) Schematic representation of sucrose separation of polysomes.

(C) Absorbance at 260 nm for all aligned polysome fractions (1–13). Values for HCT116 control cells or KDM5A knockout (KO) cells are shown as green or pink lines, respectively.

(D) Distribution of *TP53* mRNA in each fraction of the polysome profile of either HCT116 control cells (green) or KDM5A-KO cells (pink). Values are represented as a percentage of *TP53* mRNA for a single fraction and as a percentage of the total *TP53* mRNA across all fractions. Data are mean ± SEM.

(E) The steady-state *TP53* mRNA levels from control and KDM5A-KO input samples compared with 18S RNA. Technical triplicates for each were performed.

(F) Schematic representation for Click-iT metabolic labeling of newly synthesized proteins.

(G) AHA-labeled cells underwent the "Click-iT" either with or without biotin added. Increased biotinylated p53 is shown compared with total p53 protein immunoprecipitated (upper panel). Western blot analysis of input samples before immunoprecipitation (lower panel). Biotin or p53 band intensity in KDM5A knockout cells was quantified by ImageJ and normalized to controls.

(H) Total biotinylated protein comparing KDM5A-KO cells and control cells. Intensity of the biotin bands were quantified by ImageJ and normalized to loading control.

p53 proteins, including old (non-labeled) and new (labeled) proteins, are immunoprecipitated, followed by immunoblotting for biotin and p53. The biotin antibody only detects newly synthesized p53 that was pulled down. Consistent with S^{35} radioactive labeling, the Click-iT labeling assay also showed that p53 protein synthesis was increased by KDM5A knockout (Figure 6G). However, the total new proteins were not affected by KDM5A

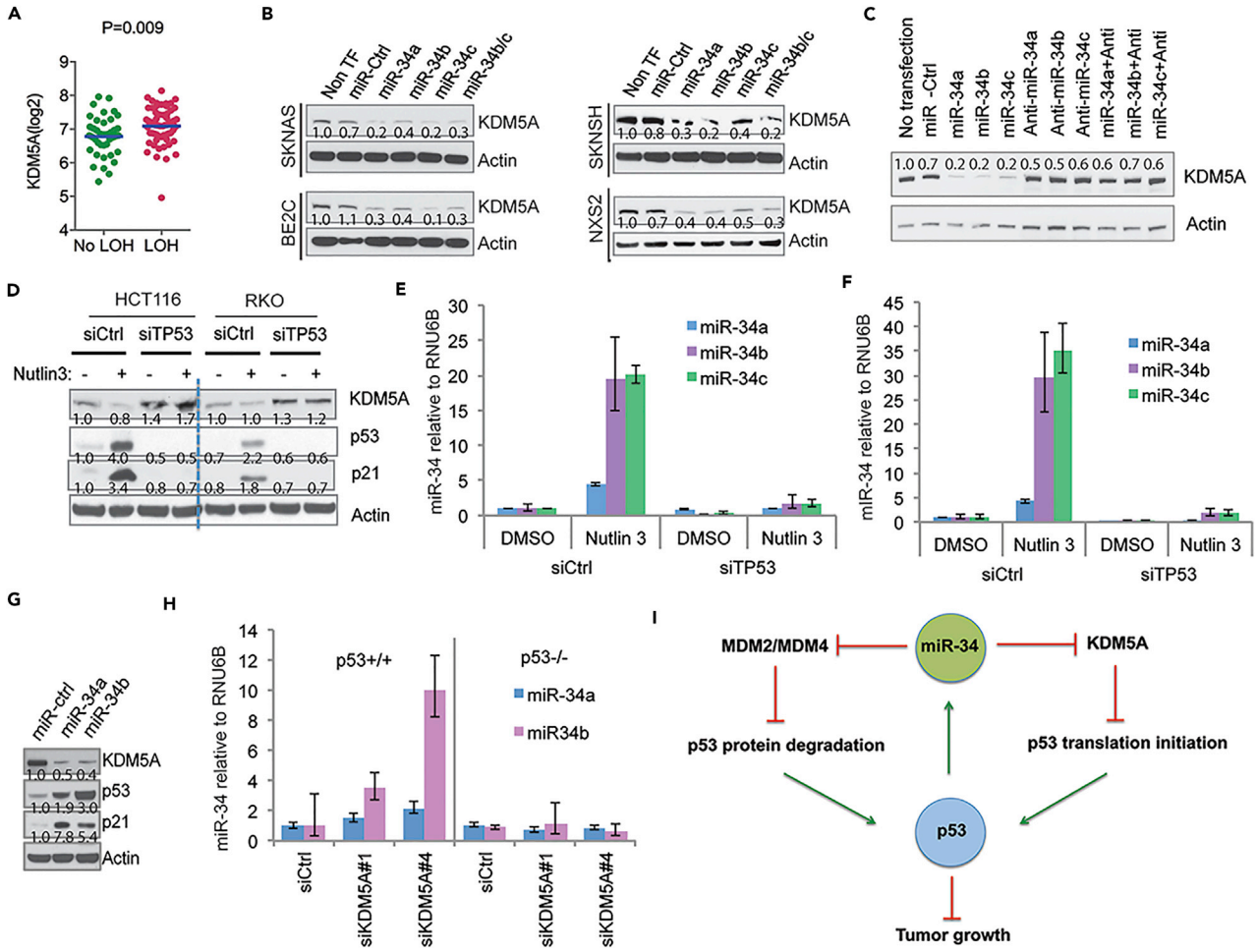

Figure 7. A Regulatory Feedback Loop between miR-34 and KDM5A

(A) The association of KDM5A gene expression in neuroblastomas (GSE3960 dataset) with LOH of 1p36 and/or 11q23 analyzed by Student's t test in the Prism program.

(B) Western blot assessing KDM5A expression in neuroblastoma cells transfected with miR-34 precursors for 72 hr. Band intensity was quantified by ImageJ and normalized to loading control.

(C) BE2(C) cells were transfected with miR-34 and anti-miRs for western blot analysis. Band intensity was quantified by ImageJ and normalized to loading control.

(D) HCT116 and RKO cells were transfected with p53 siRNA, followed by 48 hr of 5 μM Nutlin-3 treatment and analyzed by western blot. Band intensity was quantified by ImageJ and normalized to loading control.

(E and F) RT-PCR analysis of miR-34 expression in HCT116 (E) and RKO (F) from the same experiment as (D). Data are mean ± SEM.

(G) Western blot analysis of p53 and KDM5A expression after 72-hr transfection of miR-34. Band intensity was quantified by ImageJ and normalized to loading control.

(H) RT-PCR to assess miR-34 expression in isogenic $p53^{+/+}$ and $p53^{-/-}$ HCT116 cells 48 hr after siRNA-mediated knockdown of KDM5A. Data are mean ± SEM.

(I) A working model of the interactions between the KDM5A and p53 signaling pathways.

deletion (Figure 6H), similar to what we have seen previously (Figure 4E). These data indicate that KDM5A specifically regulates p53 protein translation by modulating its mRNA protein synthesis.

miR-34 Inhibits KDM5A Expression

Despite the importance of KDM5A, how it is regulated in cells is not clear. To determine what genetic factors might, in turn, regulate KDM5A expression, we analyzed published neuroblastoma microarray datasets with well-characterized genetic lesions and found that upregulation of KDM5A is correlated with loss of heterozygosity (LOH) of 1p36 and 11q23 in patients with neuroblastoma (Figure 7A). Interestingly,

members of the miR-34 family of microRNAs (miRNAs), known to be direct targets of p53 (He et al., 2007) and mimics of which were being tested in a clinical trial for hepatocellular carcinoma, reside within these regions; miR-34a is located on chromosome 1p36, whereas its paralogs, the miR-34b/c cluster, is located on chromosome 11q23. LOH or silencing in either or both of these regions is common in a variety of human cancers (Bader, 2012), including neuroblastoma (Attiyeh et al., 2005), suggesting that these miRNAs may have a critical role in oncogenesis as tumor suppressors (Bader, 2012). To assess the functional link between miR-34 and KDM5A, we introduced miR-34 precursors into several neuroblastoma cell lines. Western blot analysis on protein from transfected cells showed that expression of KDM5A was downregulated by miR-34, suggesting that miR-34 targets KDM5A (Figure 7B). To further confirm the specificity of miR-34 in the regulation of KDM5A expression, we used an anti-miR to block miR-34 function, resulting in rescue of the expression of KDM5A (Figure 7C). The BE2(C) cell line has no detectable miR-34 expression (data not shown), and thus, introduction of anti-miR-34 into these cells has little effect on KDM5A expression.

To determine whether the induction of miR-34, through activation of p53, was able to recapitulate the signature of direct introduction of miR-34 precursors, HCT116 and RKO cells were treated with Nutlin-3 or doxorubicin (Figures 7D and S4A). Induction of p53 resulted in upregulation of miR-34 (Figures 7E and 7F) and concomitantly, downregulation of KDM5A (Figure 7D). Importantly, this was p53 dependent as depletion of p53 rescued the phenotype (Figures 7D–7F). We also found that activation of p53 in the neuroblastoma cell line NB-1691 caused upregulation of miR-34, but knockdown of p53 in these cells diminished these effects (Figure S4B), indicating a general mechanism. Importantly, introduction of miR-34 into HCT116 cells significantly upregulated p53 expression (Figure 7G). These data support our findings that miR-34 targets KDM5A through a p53-dependent process and suggest that a feedback loop exists. Indeed, KDM5A also regulated miR-34 in a p53-dependent manner with KDM5A knockdown resulting in miR-34 induction in $p53^{+/+}$ but not in $p53^{-/-}$ cells (Figure 7H). Moreover, genes regulated by KDM5A were significantly enriched in the miR-34b/c signature revealed by GSEA analysis, further supporting the relationship between miR-34 and KDM5A (Figure S4C). In addition, we confirmed that KDM5B, another member of KDM5 family, was not affected by either doxorubicin or p53 knockdown (Figure S4D), indicating that KDM5A is specifically involved in the p53 pathway.

DISCUSSION

p53 is commonly mutated in many different types of cancer. In addition, the classical p14Arf-MDM2 pathway plays an important role in regulating p53 protein expression (Kamijo et al., 1998; Stott et al., 1998; Zhang et al., 1998); this pathway is frequently deregulated in cancer. Nevertheless, some types of cancers such as neuroblastoma rarely bear p53 somatic mutations or alterations of the p14Arf-MDM2 pathway (Molenaar et al., 2012; Pugh et al., 2013), indicating that other mechanisms may exist that suppress p53 function in these cancers (Veschi et al., 2017). With the identification of the first true histone demethylase KDM1A/LSD1 (Shi et al., 2004), which is able to modulate p53 methylation, another class of JmjC histone demethylases has been shown to be deregulated in multiple cancers (Kandoth et al., 2013). However, the roles and working mechanisms of these histone demethylases in cancer have not been fully characterized. In this study, we identified several histone demethylases (KDM4D, KDM5A, KDM6B, PHF2, PHF8) and two additional JmjC-domain-containing proteins (C14orf169 and JMJD4) that are involved in regulating p53 activity. KDM4D is an H3K9me3/me2 demethylase and is able to induce p21 expression (Kim et al., 2012). However, overexpression of KDM4D causes global demethylation of H3K9me3, which may result in DNA damage and subsequent p53 activation. Similarly, loss of KDM4D may also result in a DNA damage response (Khoury-Haddad et al., 2015), and thus, activation of p53. KDM6B is an H3K27me3/me2 demethylase and can be recruited to p53-bound promoters and enhancer elements with unknown function (Williams et al., 2014). It is possible that KDM6B suppresses p53 function in this scenario. Although the histone demethylase activity of PHF2 is not definite, it has been shown to facilitate p53-mediated cell death in response to chemotherapy (Lee et al., 2014). PHF8 is an H3K9me2/me1 and H4K20me1 demethylase, but how it regulates p53 activity needs further studies. C14orf169 and JMJD4 may not have histone demethylase activity, and no previous studies show that they are involved in p53 function.

Although most genetic mutations in the coding sequences of *TP53* disrupt the functions of p53, a rare polymorphism (rs78378222) in the 3′-UTR of *TP53*, which affects p53 protein translation, was found to confer susceptibility to multiple cancers, including neuroblastoma (Diskin et al., 2014; Stacey et al., 2011). These data suggest that repression of p53 protein translation contributes to oncogenesis. Here we found that the histone demethylase KDM5A was amplified in many types of cancers, and this was negatively correlated with

TP53 mutation when compared with KDM5A loss. Most interestingly, we found that KDM5A regulates p53 function by inhibiting p53 protein translation, which may explain why KDM5A amplification is negatively correlated with *TP53* mutation. A previous study had shown that ribosomal protein L26 (RPL26) and nucleolin could bind the 5′-UTR of p53 mRNA to control p53 translation and induction after DNA damage (Takagi et al., 2005). RNPC1 has been reported to repress p53 translation in lymphomas (Zhang et al., 2011). However, our data did not show a significant change in RNPC1, RPL26, or nucleolin expression after depletion of KDM5A, and loss of KDM5A did not induce a significant DNA damage response as assessed by measuring phosphorylated p53, suggesting that KDM5A works through a different mechanism. Indeed, KDM5A negatively regulated a subgroup of genes that are involved in translation initiation such as EIF5A and EIF2B4. Since depletion or knockout of KDM5A had no effect on global protein synthesis based on the assessment of newly synthesized proteins by using S^{35} labeling (Figure 4E) and Click-iT labeling technology (Figure 6), we speculate that two possible mechanisms (which are not mutually exclusive) may account for p53 synthesis regulated by KDM5A: (1) KDM5A regulates a specific program that alters the stoichiometry of translational complex components such as EIF2B4, leading to the activation of a specific translation machinery that promotes p53 synthesis. (2) Specific secondary structures of *TP53* mRNA, as reported previously (Candeias et al., 2008; Fu et al., 1996; Ray et al., 2006), respond to the translation machinery induced by KDM5A. However, other additional mechanisms may exist; hence more studies are needed. In addition, whether there are other mRNAs whose translation is subject to KDM5A knockdown needs to be determined in the future.

Interestingly, by mining a database of a genome-scale genetic interaction map in yeast (Costanzo et al., 2010), we found that there was a positive genetic interaction between *TIF5* and *JHD2*, the homologs of *eIF5* and *KDM5A* in mammals; that is, the phenotype of *TIF5* mutant was partially rescued by *JHD2* mutation. Translation initiation factor eIF5 functions to regulate eIF2 activity. Although yeast does not have the p53 tumor suppressor gene, this may indicate that there is an evolutionarily conserved function for KDM5A in the regulation of protein translation. Consistent with the regulatory mechanism of KDM5A, expression of mutant p53 is also enhanced by loss of KDM5A. Mutation in p53 can be seen as a late event in multiple recurrent, chemotherapy-resistant cancers such as neuroblastoma (Keshelava et al., 2000), and mutant p53 may have additional, direct oncogenic actions that are different from the results of inhibiting p53 signaling early on in tumor progression (Muller and Vousden, 2014). Considering the context-dependent features of epigenetic modifiers in cancer, under some circumstances, loss of function of KDM5A might afford an additional growth advantage to affected cells with mutant p53. Despite the observation that *KDM5A* amplification tends to be mutually exclusive to *TP53* mutation, there were a fraction of tumors showing co-occurrence of *KDM5A* amplification and *TP53* mutation. This may suggest that either KDM5A has p53-independent function or that amplification of *KDM5A* confers selective pressure on p53, leading to p53 mutation during cancer progression. Nevertheless, genetic deletion of *p14Arf* and amplification of *MDM2*, two classical modulators of p53, also frequently overlap with *TP53* mutations.

Although the mechanism by which KDM5A regulates the expression of its targets needs a deeper understanding, we found that KDM5A was located in the promoter regions of its downstream targets from both our own ChIP-seq data and ENCODE data and correlated with changes of the H3K4me3 mark, which is representative of active gene transcription. These data indicate that KDM5A directly regulates the expression of these genes. Previous studies also show that KDM5A can exert biological functions in a histone-demethylase-independent manner (Cao et al., 2014; DiTacchio et al., 2011; Secombe and Eisenman, 2007). Whether KDM5A regulates p53 translation through its histone demethylase activity needs to be further addressed in the future by using a potent and specific inhibitor.

Although p53 significantly induces p21 after KDM5A depletion, interestingly, we observed some induction of p21 expression in p53-null cells after the loss of KDM5A. The mechanism for this also needs to be further investigated. A recent study shows that KDM5A interacts with the nucleosome remodeling and deacetylase (NuRD) complex (Nishibuchi et al., 2014), which usually exerts gene repressive functions (Denslow and Wade, 2007), and HDAC is one of the core components of the NuRD complex (Denslow and Wade, 2007). It is well known that HDAC inhibitors induce p21 expression (Gui et al., 2004), so we speculate that KDM5A may modulate HDAC activity to suppress p21 induction, regardless of the p53 status.

We also found that miR-34s (transcriptional targets of p53) target KDM5A expression (Figure 7). A recent study showed that miR-34 targets MDM4 (Okada et al., 2014), which facilities MDM2-mediated

function, resulting in p53 stabilization. Thus, miR-34 seems to bridge p53 protein stability and translation, thereby enhancing p53 activity (Figure 6I). Although this might suggest a feedback loop among these molecules, studies need to delve into more depth to consolidate this interesting observation.

In summary, we have identified a mechanism by which the histone demethylase KDM5A regulates p53 expression by modulating its translation initiation. Targeting KDM5A might be an option for treating p53 wild-type cancers.

Limitations of the Study

Our study has several limitations. First, the mechanism by which KDM5A affects the expression of a set of mRNA translation factors that controls p53 synthesis needs to be further investigated. Second, other messenger RNAs, in addition to p53, are likely to be regulated by KDM5A at the translational level; this needs to be investigated in future studies. In addition, the lack of a specific small-molecule KDM5A inhibitor prevents additional validation of the effect of KDM5A inhibition on tumor growth in the xenograft model. Last, the regulation of KDM5A by miR-34 also needs further in-depth studies to understand the upregulation of p53 by miR-34.

METHODS

All methods can be found in the accompanying Transparent Methods supplemental file.

DATA AND SOFTWARE AVAILABILITY

All microarray and deep sequencing data have been deposited in GEO under accession number: GSE45967, GSE49854, GSE100511, GSE107221.

SUPPLEMENTAL INFORMATION

Supplemental Information includes Transparent Methods, four figures, and seven tables and can be found with this article online at https://doi.org/10.1016/j.isci.2018.10.012.

ACKNOWLEDGMENTS

We thank William G. Kaelin, Jr., and Douglas R. Green for providing reagents and helpful discussion. We thank Bert Volgelstein and Michael Kastan for providing cell lines. We thank The Hartwell Center at St. Jude for ChIP-seq and Xenograft Core Facility for the pilot xenograft experiments. This work was supported by the Assisi Foundation of Memphis, the American Lebanese Syrian Associated Charities (ALSAC), the US Public Health Service Childhood Solid Tumor Program Project Grant No. CA23099, the Cancer Center Support Grant No. 21766 from the National Cancer Institute (A.M.D.), American Cancer Society-Research Scholar 130421-RSG-17-071-01-TBG (J.Y.), National Cancer Institute of the National Institutes of Health under Award Number R03CA212802 and R01CA229739 (J.Y.), and a Department of Defense Peer Reviewed Cancer Research Program Career Development Award W81XWH-13-1-0235 (Q.Y.). The K.M.M. laboratory is supported by the NIH National Cancer Institute (R01CA198279 and R01CA201268).

AUTHOR CONTRIBUTIONS

Conceptualization: J.Y. and A.M.D.; Methodology: J.Y., P.-H.C., D.H., and C.J.; Investigation: J.Y., P.-H.C., H.D., C.J., A.A., N.G., A.A.Z., and D.Y.; Writing – Original Draft: J.Y.; Writing –Review & Editing: A.M.D., Q.Y., T.C., G.P.Z., Y.W, B.S., and C.L.; Formal Analysis: G.K., L.P., and Y.F.; Resources: R.C.K., K.M.M., Q.Y., Y.W., C.L., M.B., T.C.; Supervision: J.Y., A.M.D.; Funding Acquisition: J.Y., A.M.D., and K.M.

DECLARATION OF INTERESTS

The authors declare no competing interests.

Received: January 23, 2018
Revised: September 1, 2018
Accepted: October 10, 2018
Published: November 30, 2018

REFERENCES

Attiyeh, E.F., London, W.B., Mosse, Y.P., Wang, Q., Winter, C., Khazi, D., McGrady, P.W., Seeger, R.C., Look, A.T., Shimada, H., et al. (2005). Chromosome 1p and 11q deletions and outcome in neuroblastoma. N. Engl. J. Med. *353*, 2243–2253.

Bader, A.G. (2012). miR-34-a microRNA replacement therapy is headed to the clinic. Front Genet. *3*, 120.

Banelli, B., Carra, E., Barbieri, F., Wurth, R., Parodi, F., Pattarozzi, A., Carosio, R., Forlani, A., Allemanni, G., Marubbi, D., et al. (2015). The histone demethylase KDM5A is a key factor for the resistance to temozolomide in glioblastoma. Cell Cycle *14*, 3418–3429.

Beroukhim, R., Mermel, C.H., Porter, D., Wei, G., Raychaudhuri, S., Donovan, J., Barretina, J., Boehm, J.S., Dobson, J., Urashima, M., et al. (2010). The landscape of somatic copy-number alteration across human cancers. Nature *463*, 899–905.

Bhat, M., Robichaud, N., Hulea, L., Sonenberg, N., Pelletier, J., and Topisirovic, I. (2015). Targeting the translation machinery in cancer. Nat. Rev. Drug Discov. *14*, 261–278.

Blair, L.P., Cao, J., Zou, M.R., Sayegh, J., and Yan, Q. (2011). Epigenetic regulation by lysine demethylase 5 (KDM5) enzymes in cancer. Cancers (Basel) *3*, 1383–1404.

Candeias, M.M., Malbert-Colas, L., Powell, D.J., Daskalogianni, C., Maslon, M.M., Naski, N., Bourougaa, K., Calvo, F., and Fahraeus, R. (2008). P53 mRNA controls p53 activity by managing Mdm2 functions. Nat. Cell Biol. *10*, 1098–1105.

Cao, J., Liu, Z., Cheung, W.K., Zhao, M., Chen, S.Y., Chan, S.W., Booth, C.J., Nguyen, D.X., and Yan, Q. (2014). Histone demethylase RBP2 is critical for breast cancer progression and metastasis. Cell Rep. *6*, 868–877.

Cencic, R., Hall, D.R., Robert, F., Du, Y., Min, J., Li, L., Qui, M., Lewis, I., Kurtkaya, S., Dingledine, R., et al. (2011). Reversing chemoresistance by small molecule inhibition of the translation initiation complex eIF4F. Proc. Natl. Acad. Sci. U S A *108*, 1046–1051.

Cerami, E., Gao, J., Dogrusoz, U., Gross, B.E., Sumer, S.O., Aksoy, B.A., Jacobsen, A., Byrne, C.J., Heuer, M.L., Larsson, E., et al. (2012). The cBio cancer genomics portal: an open platform for exploring multidimensional cancer genomics data. Cancer Discov. *2*, 401–404.

Chi, P., Allis, C.D., and Wang, G.G. (2010). Covalent histone modifications–miswritten, misinterpreted and mis-erased in human cancers. Nat. Rev. Cancer *10*, 457–469.

Christensen, J., Agger, K., Cloos, P.A., Pasini, D., Rose, S., Sennels, L., Rappsilber, J., Hansen, K.H., Salcini, A.E., and Helin, K. (2007). RBP2 belongs to a family of demethylases, specific for tri-and dimethylated lysine 4 on histone 3. Cell *128*, 1063–1076.

Costanzo, M., Baryshnikova, A., Bellay, J., Kim, Y., Spear, E.D., Sevier, C.S., Ding, H., Koh, J.L., Toufighi, K., Mostafavi, S., et al. (2010). The genetic landscape of a cell. Science *327*, 425–431.

Dawson, M.A., and Kouzarides, T. (2012). Cancer epigenetics: from mechanism to therapy. Cell *150*, 12–27.

de Rooij, J.D., Hollink, I.H., Arentsen-Peters, S.T., van Galen, J.F., Berna Beverloo, H., Baruchel, A., Trka, J., Reinhardt, D., Sonneveld, E., Zimmermann, M., et al. (2013). NUP98/JARID1A is a novel recurrent abnormality in pediatric acute megakaryoblastic leukemia with a distinct HOX gene expression pattern. Leukemia *27*, 2280–2288.

Denslow, S.A., and Wade, P.A. (2007). The human Mi-2/NuRD complex and gene regulation. Oncogene *26*, 5433–5438.

Didiot, M.C., Hewett, J., Varin, T., Freuler, F., Selinger, D., Nick, H., Reinhardt, J., Buckler, A., Myer, V., Schuffenhauer, A., et al. (2013). Identification of cardiac glycoside molecules as inhibitors of c-Myc IRES-mediated translation. J. Biomol. Screen. *18*, 407–419.

Diskin, S.J., Capasso, M., Diamond, M., Oldridge, D.A., Conkrite, K., Bosse, K.R., Russell, M.R., Iolascon, A., Hakonarson, H., Devoto, M., et al. (2014). Rare variants in TP53 and susceptibility to neuroblastoma. J. Natl. Cancer Inst. *106*, dju047.

DiTacchio, L., Le, H.D., Vollmers, C., Hatori, M., Witcher, M., Secombe, J., and Panda, S. (2011). Histone lysine demethylase JARID1a activates CLOCK-BMAL1 and influences the circadian clock. Science *333*, 1881–1885.

Fu, L., Minden, M.D., and Benchimol, S. (1996). Translational regulation of human p53 gene expression. EMBO J. *15*, 4392–4401.

Gao, J., Aksoy, B.A., Dogrusoz, U., Dresdner, G., Gross, B., Sumer, S.O., Sun, Y., Jacobsen, A., Sinha, R., Larsson, E., et al. (2013). Integrative analysis of complex cancer genomics and clinical profiles using the cBioPortal. Sci. Signal. *6*, pl1.

Greer, E.L., and Shi, Y. (2012). Histone methylation: a dynamic mark in health, disease and inheritance. Nat. Rev. Genet. *13*, 343–357.

Gui, C.Y., Ngo, L., Xu, W.S., Richon, V.M., and Marks, P.A. (2004). Histone deacetylase (HDAC) inhibitor activation of p21WAF1 involves changes in promoter-associated proteins, including HDAC1. Proc. Natl. Acad. Sci. U S A *101*, 1241–1246.

He, L., He, X., Lim, L.P., de Stanchina, E., Xuan, Z., Liang, Y., Xue, W., Zender, L., Magnus, J., Ridzon, D., et al. (2007). A microRNA component of the p53 tumour suppressor network. Nature *447*, 1130–1134.

Hou, J., Wu, J., Dombkowski, A., Zhang, K., Holowatyj, A., Boerner, J.L., and Yang, Z.Q. (2012). Genomic amplification and a role in drug-resistance for the KDM5A histone demethylase in breast cancer. Am. J. Transl. Res. *4*, 247–256.

Huang, J., Sengupta, R., Espejo, A.B., Lee, M.G., Dorsey, J.A., Richter, M., Opravil, S., Shiekhattar, R., Bedford, M.T., Jenuwein, T., et al. (2007). p53 is regulated by the lysine demethylase LSD1. Nature *449*, 105–108.

Kaelin, W.G., Jr., and McKnight, S.L. (2013). Influence of metabolism on epigenetics and disease. Cell *153*, 56–69.

Kamijo, T., Weber, J.D., Zambetti, G., Zindy, F., Roussel, M.F., and Sherr, C.J. (1998). Functional and physical interactions of the ARF tumor suppressor with p53 and Mdm2. Proc. Natl. Acad. Sci. U S A *95*, 8292–8297.

Kandoth, C., McLellan, M.D., Vandin, F., Ye, K., Niu, B., Lu, C., Xie, M., Zhang, Q., McMichael, J.F., Wyczalkowski, M.A., et al. (2013). Mutational landscape and significance across 12 major cancer types. Nature *502*, 333–339.

Keshelava, N., Zuo, J.J., Waidyaratne, N.S., Triche, T.J., and Reynolds, C.P. (2000). p53 mutations and loss of p53 function confer multidrug resistance in neuroblastoma. Med. Pediatr. Oncol. *35*, 563–568.

Kessis, T.D., Slebos, R.J., Nelson, W.G., Kastan, M.B., Plunkett, B.S., Han, S.M., Lorincz, A.T., Hedrick, L., and Cho, K.R. (1993). Human papillomavirus 16 E6 expression disrupts the p53-mediated cellular response to DNA damage. Proc. Natl. Acad. Sci. U S A *90*, 3988–3992.

Khoury-Haddad, H., Nadar-Ponniah, P.T., Awwad, S., and Ayoub, N. (2015). The emerging role of lysine demethylases in DNA damage response: dissecting the recruitment mode of KDM4D/JMJD2D to DNA damage sites. Cell Cycle *14*, 950–958.

Kim, T.D., Oh, S., Shin, S., and Janknecht, R. (2012). Regulation of tumor suppressor p53 and HCT116 cell physiology by histone demethylase JMJD2D/KDM4D. PLoS One *7*, e34618.

Klose, R.J., Yan, Q., Tothova, Z., Yamane, K., Erdjument-Bromage, H., Tempst, P., Gilliland, D.G., Zhang, Y., and Kaelin, W.G., Jr. (2007). The retinoblastoma binding protein RBP2 is an H3K4 demethylase. Cell *128*, 889–900.

Kooistra, S.M., and Helin, K. (2012). Molecular mechanisms and potential functions of histone demethylases. Nat. Rev. Mol. Cell Biol *13*, 297–311.

Kruse, J.P., and Gu, W. (2009). Modes of p53 regulation. Cell *137*, 609–622.

Lane, D., and Levine, A. (2010). p53 Research: the past thirty years and the next thirty years. Cold Spring Harb. Perspect. Biol. *2*, a000893.

Lee, K.H., Park, J.W., Sung, H.S., Choi, Y.J., Kim, W.H., Lee, H.S., Chung, H.J., Shin, H.W., Cho, C.H., Kim, T.Y., et al. (2014). PHF2 histone demethylase acts as a tumor suppressor in association with p53 in cancer. Oncogene *34*, 2897–2909.

Levine, A.J., and Oren, M. (2009). The first 30 years of p53: growing ever more complex. Nat. Rev. Cancer *9*, 749–758.

Li, L., Wang, L., Song, P., Geng, X., Liang, X., Zhou, M., Wang, Y., Chen, C., Jia, J., and Zeng, J. (2014). Critical role of histone demethylase RBP2 in human gastric cancer angiogenesis. Mol. Cancer *13*, 81.

Lin, W., Cao, J., Liu, J., Beshiri, M.L., Fujiwara, Y., Francis, J., Cherniack, A.D., Geisen, C., Blair, L.P., Zou, M.R., et al. (2011). Loss of the retinoblastoma binding protein 2 (RBP2) histone demethylase suppresses tumorigenesis in mice lacking Rb1 or Men1. Proc. Natl. Acad. Sci. U S A *108*, 13379–13386.

Maris, J.M. (2010). Recent advances in neuroblastoma. N. Engl. J. Med. *362*, 2202–2211.

Molenaar, J.J., Koster, J., Zwijnenburg, D.A., van Sluis, P., Valentijn, L.J., van der Ploeg, I., Hamdi, M., van Nes, J., Westerman, B.A., van Arkel, J., et al. (2012). Sequencing of neuroblastoma identifies chromothripsis and defects in neuritogenesis genes. Nature *483*, 589–593.

Muller, P.A., and Vousden, K.H. (2014). Mutant p53 in cancer: new functions and therapeutic opportunities. Cancer Cell *25*, 304–317.

Nishibuchi, G., Shibata, Y., Hayakawa, T., Hayakawa, N., Ohtani, Y., Sinmyozu, K., Tagami, H., and Nakayama, J. (2014). Physical and functional interactions between the histone H3K4 demethylase KDM5A and the nucleosome remodeling and deacetylase (NuRD) complex. J. Biol. Chem. *289*, 28956–28970.

Okada, N., Lin, C.P., Ribeiro, M.C., Biton, A., Lai, G., He, X., Bu, P., Vogel, H., Jablons, D.M., Keller, A.C., et al. (2014). A positive feedback between p53 and miR-34 miRNAs mediates tumor suppression. Genes Dev. *28*, 438–450.

Pugh, T.J., Morozova, O., Attiyeh, E.F., Asgharzadeh, S., Wei, J.S., Auclair, D., Carter, S.L., Cibulskis, K., Hanna, M., Kiezun, A., et al. (2013). The genetic landscape of high-risk neuroblastoma. Nat. Genet. *45*, 279–284.

Qi, L., Zhu, F., Li, S.H., Si, L.B., Hu, L.K., and Tian, H. (2014). Retinoblastoma binding protein 2 (RBP2) promotes HIF-1alpha-VEGF-induced angiogenesis of non-small cell lung cancer via the Akt pathway. PLoS One *9*, e106032.

Ray, P.S., Grover, R., and Das, S. (2006). Two internal ribosome entry sites mediate the translation of p53 isoforms. EMBO Rep. *7*, 404–410.

Rees, M.G., Seashore-Ludlow, B., Cheah, J.H., Adams, D.J., Price, E.V., Gill, S., Javaid, S., Coletti, M.E., Jones, V.L., Bodycombe, N.E., et al. (2016). Correlating chemical sensitivity and basal gene expression reveals mechanism of action. Nat. Chem. Biol. *12*, 109–116.

Rodrigo, C.M., Cencic, R., Roche, S.P., Pelletier, J., and Porco, J.A. (2012). Synthesis of rocaglamide hydroxamates and related compounds as eukaryotic translation inhibitors: synthetic and biological studies. J. Med. Chem. *55*, 558–562.

Secombe, J., and Eisenman, R.N. (2007). The function and regulation of the JARID1 family of histone H3 lysine 4 demethylases: the Myc connection. Cell Cycle *6*, 1324–1328.

Sharma, S.V., Lee, D.Y., Li, B., Quinlan, M.P., Takahashi, F., Maheswaran, S., McDermott, U., Azizian, N., Zou, L., Fischbach, M.A., et al. (2010). A chromatin-mediated reversible drug-tolerant state in cancer cell subpopulations. Cell *141*, 69–80.

Shi, Y., Lan, F., Matson, C., Mulligan, P., Whetstine, J.R., Cole, P.A., Casero, R.A., and Shi, Y. (2004). Histone demethylation mediated by the nuclear amine oxidase homolog LSD1. Cell *119*, 941–953.

Stacey, S.N., Sulem, P., Jonasdottir, A., Masson, G., Gudmundsson, J., Gudbjartsson, D.F., Magnusson, O.T., Gudjonsson, S.A., Sigurgeirsson, B., Thorisdottir, K., et al. (2011). A germline variant in the TP53 polyadenylation signal confers cancer susceptibility. Nat. Genet. *43*, 1098–1103.

Stott, F.J., Bates, S., James, M.C., McConnell, B.B., Starborg, M., Brookes, S., Palmero, I., Ryan, K., Hara, E., Vousden, K.H., et al. (1998). The alternative product from the human CDKN2A locus, p14(ARF), participates in a regulatory feedback loop with p53 and MDM2. EMBO J. *17*, 5001–5014.

Su, Z., Fang, H., Hong, H., Shi, L., Zhang, W., Zhang, W., Zhang, Y., Dong, Z., Lancashire, L.J., Bessarabova, M., et al. (2014). An investigation of biomarkers derived from legacy microarray data for their utility in the RNA-seq era. Genome Biol. *15*, 523.

Suva, M.L., Riggi, N., and Bernstein, B.E. (2013). Epigenetic reprogramming in cancer. Science *339*, 1567–1570.

Takagi, M., Absalon, M.J., McLure, K.G., and Kastan, M.B. (2005). Regulation of p53 translation and induction after DNA damage by ribosomal protein L26 and nucleolin. Cell *123*, 49–63.

Teng, Y.C., Lee, C.F., Li, Y.S., Chen, Y.R., Hsiao, P.W., Chan, M.Y., Lin, F.M., Huang, H.D., Chen, Y.T., Jeng, Y.M., et al. (2013). Histone demethylase RBP2 promotes lung tumorigenesis and cancer metastasis. Cancer Res. *73*, 4711–4721.

Toledo, F., and Wahl, G.M. (2006). Regulating the p53 pathway: in vitro hypotheses, in vivo veritas. Nat. Rev. Cancer *6*, 909–923.

Tweddle, D.A., Malcolm, A.J., Bown, N., Pearson, A.D., and Lunec, J. (2001). Evidence for the development of p53 mutations after cytotoxic therapy in a neuroblastoma cell line. Cancer Res. *61*, 8–13.

van Zutven, L.J., Onen, E., Velthuizen, S.C., van Drunen, E., von Bergh, A.R., van den Heuvel-Eibrink, M.M., Veronese, A., Mecucci, C., Negrini, M., de Greef, G.E., et al. (2006). Identification of NUP98 abnormalities in acute leukemia: JARID1A (12p13) as a new partner gene. Genes Chromosomes Cancer *45*, 437–446.

Veschi, V., Liu, Z., Voss, T.C., Ozbun, L., Gryder, B., Yan, C., Hu, Y., Ma, A., Jin, J., Mazur, S.J., et al. (2017). Epigenetic siRNA and chemical screens identify SETD8 inhibition as a therapeutic strategy for p53 activation in high-risk neuroblastoma. Cancer Cell *31*, 50–63.

Vogelstein, B., and Kinzler, K.W. (2004). Cancer genes and the pathways they control. Nat. Med. *10*, 789–799.

Vogelstein, B., Papadopoulos, N., Velculescu, V.E., Zhou, S., Diaz, L.A., Jr., and Kinzler, K.W. (2013). Cancer genome landscapes. Science *339*, 1546–1558.

Vousden, K.H., and Prives, C. (2009). Blinded by the light: the growing complexity of p53. Cell *137*, 413–431.

Wang, G.G., Song, J., Wang, Z., Dormann, H.L., Casadio, F., Li, H., Luo, J.L., Patel, D.J., and Allis, C.D. (2009). Haematopoietic malignancies caused by dysregulation of a chromatin-binding PHD finger. Nature *459*, 847–851.

Wang, S.J., and Gu, W. (2014). To be, or not to be: functional dilemma of p53 metabolic regulation. Curr. Opin. Oncol. *26*, 78–85.

Williams, K., Christensen, J., Rappsilber, J., Nielsen, A.L., Johansen, J.V., and Helin, K. (2014). The histone lysine demethylase JMJD3/KDM6B is recruited to p53 bound promoters and enhancer elements in a p53 dependent manner. PLoS One *9*, e96545.

Yang, J., Milasta, S., Hu, D., AlTahan, A.M., Interiano, R.B., Zhou, J., Davidson, J., Low, J., Lin, W., Bao, J., et al. (2017). Targeting histone demethylases in MYC-driven neuroblastomas with ciclopirox. Cancer Res. *77*, 4626–4638.

Zeng, Y.X., Somasundaram, K., and el-Deiry, W.S. (1997). AP2 inhibits cancer cell growth and activates p21WAF1/CIP1 expression. Nat. Genet. *15*, 78–82.

Zhang, J., Cho, S.J., Shu, L., Yan, W., Guerrero, T., Kent, M., Skorupski, K., Chen, H., and Chen, X. (2011). Translational repression of p53 by RNPC1, a p53 target overexpressed in lymphomas. Genes Dev. *25*, 1528–1543.

Zhang, Y., Xiong, Y., and Yarbrough, W.G. (1998). ARF promotes MDM2 degradation and stabilizes p53: ARF-INK4a locus deletion impairs both the Rb and p53 tumor suppression pathways. Cell *92*, 725–734.

Zitvogel, L., and Kroemer, G. (2015). CANCER. A p53-regulated immune checkpoint relevant to cancer. Science *349*, 476–477.

ISCI, Volume *9*

Supplemental Information

KDM5A Regulates a Translational Program that Controls p53 Protein Expression

Dongli Hu, Carolyn Jablonowski, Pei-Hsin Cheng, Alaa AlTahan, Chunliang Li, Yingdi Wang, Lance Palmer, Cuixia Lan, Bingmei Sun, Ahmed Abu-Zaid, Yiping Fan, Mark Brimble, Nicolas T. Gamboa, Ramhari C. Kumbhar, David Yanishevski, Kyle M. Miller, Guolian Kang, Gerard P. Zambetti, Taosheng Chen, Qin Yan, Andrew M. Davidoff, and Jun Yang

A

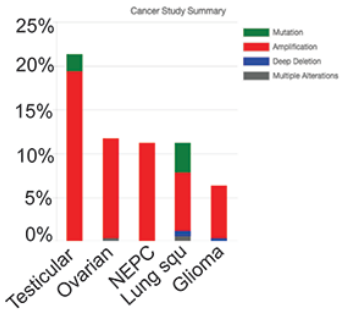

B

	NES	NOM p-val
KANNAN_TP53_TARGETS_UP	-1.2	0.162
NGA_TP53_TARGETS	-0.77	0.782
KEGG_P53_SIGNALING_PATHWAY	-1.05	0.373

C

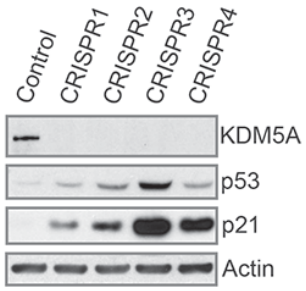

D

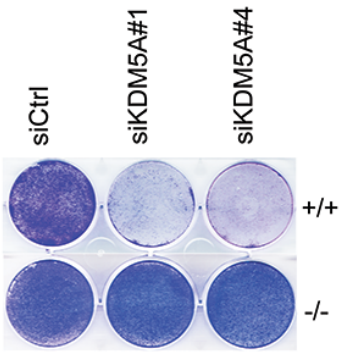

E

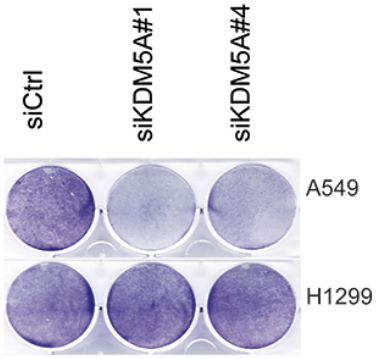

F

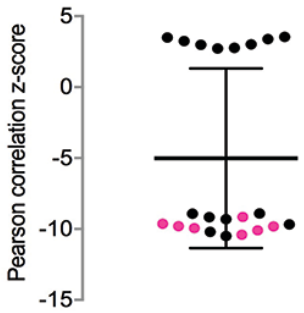

Negative correlation with drug sensitivity

BRD-K09587429
NSC30930
Austocystin D
BRD-K17060750
VAF347
ML334 diastereom
BRD-K71781559
BRD-K64610608

Positive correlation with drug sensitivity

PX-12
BRD-M60251345
Decitabine
Etoposide
PRIMA-1
BRD-M63575423
Cytarabine
BRD-M43399311
Barasertinib
KW-2449
Doxorubicin
GSK461364
Merck60
KPT185

G

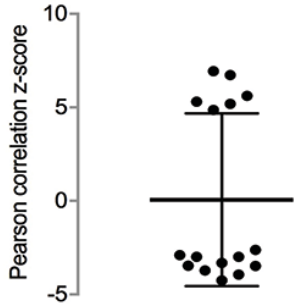

Sirolimus
Dexamethasone
BRD-M02488208
Clofarabine
Etoposide
manumycin A

Austocystin D
PD318088
BRD-M65857522
Selumetinib
Afatinib
BRD-M58862563
Vandeltanib
Nilotinib
Erlotinib
Gelfitinib

Figure S1. KDM5A regulates cell proliferation in a p53-dependent manner, related to Figures 1-3. (**A**) The genetic alterations of KDM5A in 5 different cancer cohorts for figure 2D and 2E. (**B**) GSEA analysis shows no significant enrichment of p53 signatures after KDM5A knockdown in p53-/- HCT116 cells. (**C**) Western blot for CRISPR/Cas9 knockout of KDM5A in five individual clones of p53+/+ HCT116 cells. (**D-E**) After 5-day depletion of KDM5A in p53+/+ and p53-/- HCT116 cells (D), lung cancer cell lines (E), cells were stained with crystal violet. (**F**) The correlation of KDM5A expression and drug sensitivity. Positive z-score indicates cancer cells expressing high KDM5A are resistant to the drugs while negative z-score indicates cancer cells expressing high KDM5A are sensitive to the drugs. Left lists show the top hits drug sensitivity that are either negatively or positively correlated with KDM5A expression. (**G**) Analysis of the correlation of KDM5B expression and drug sensitivity as in (F).

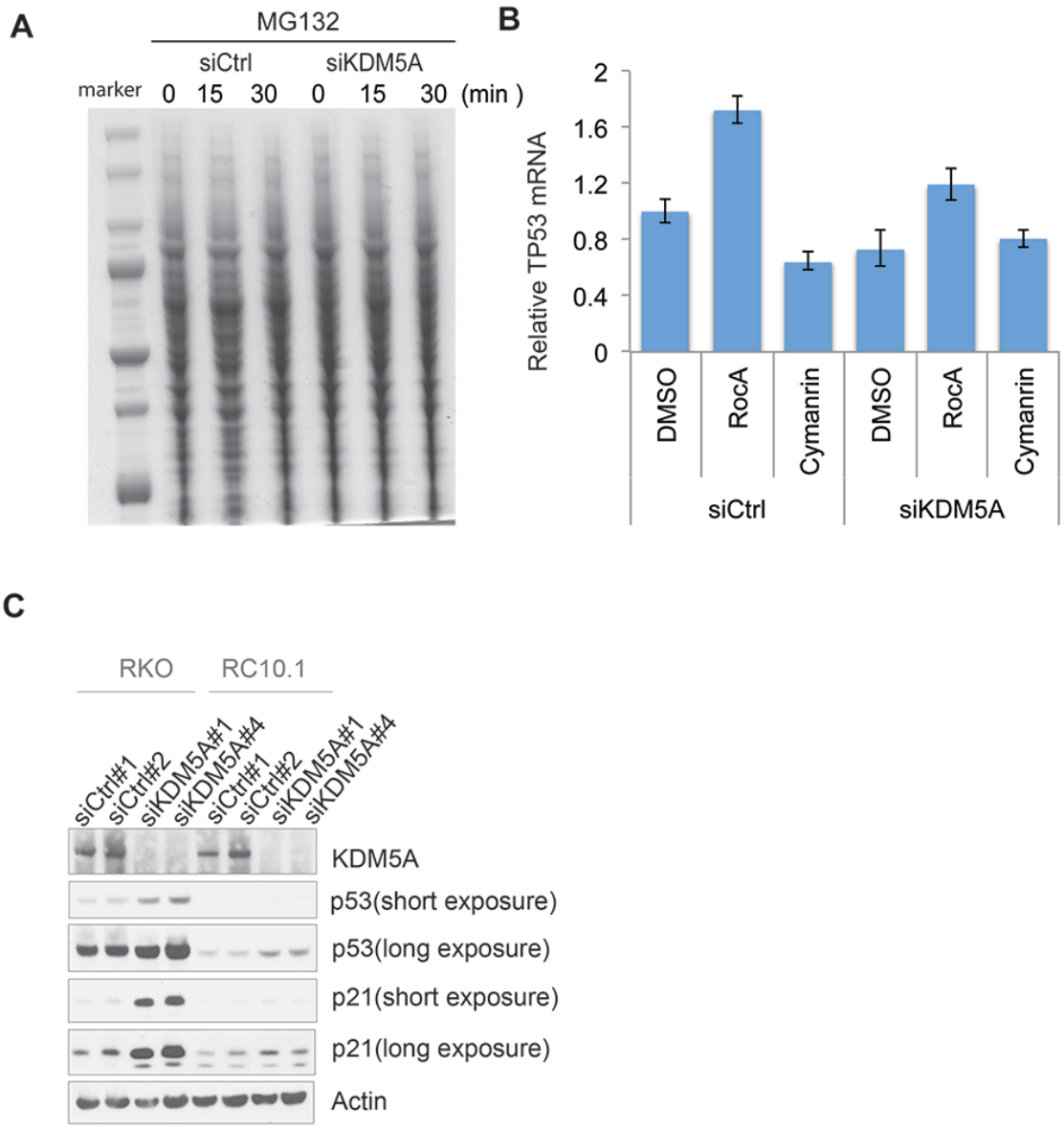

Figure S2. KDM5A regulates p53 translation, related to Figure 4.
(A) Coomassie blue staining of the total proteins for Figure 4E. **(B)** RT PCR assessment of *TP53* mRNA levels after treatment with indicated compounds of HCT116 cells. **(C**) Whole cell lysates from RKO and RC10.1 cells were blotted with the indicated antibodies after 72-hour knockdown of KDM5A.

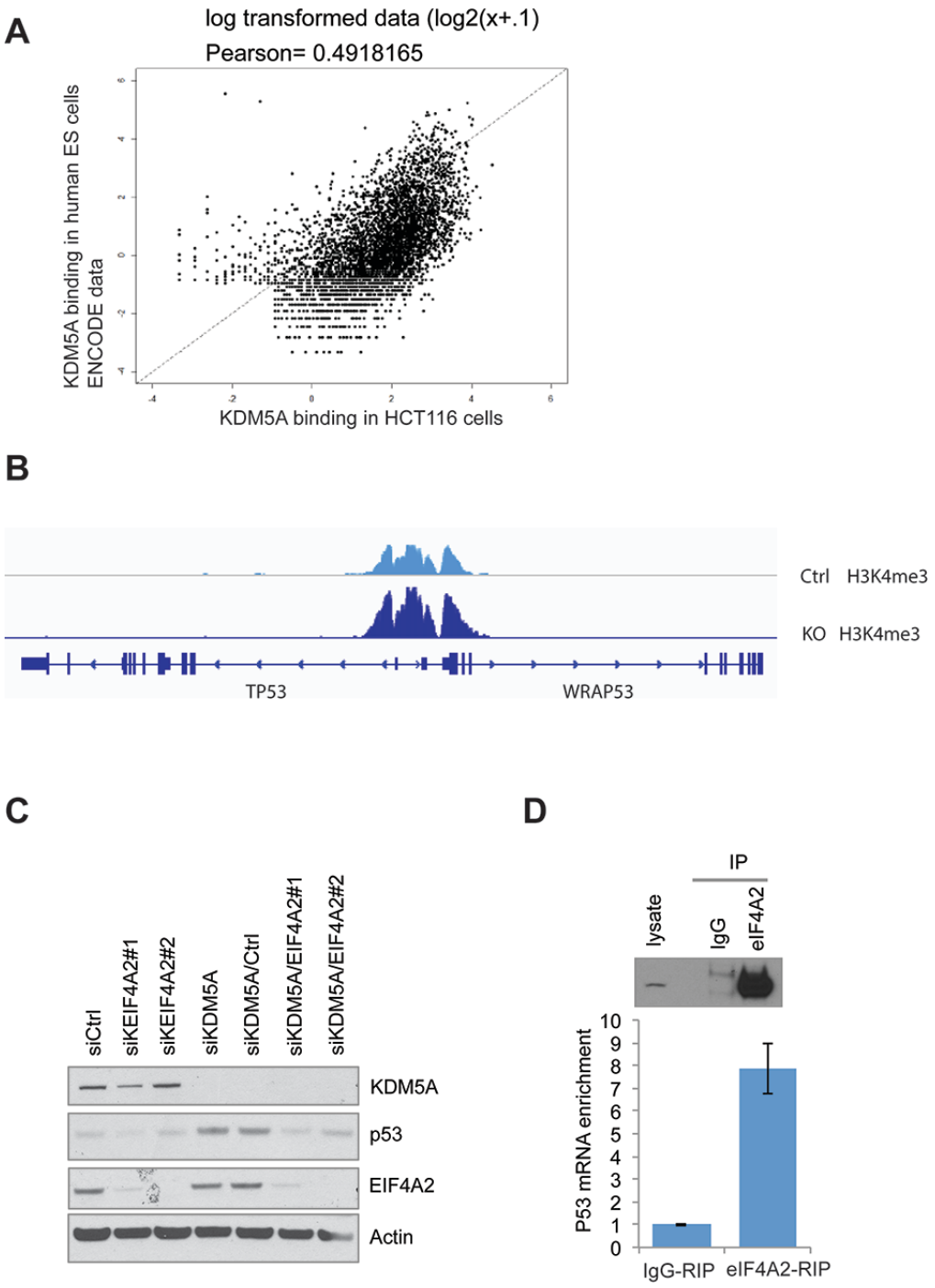

Figure S3. KDM5A regulates p53 translation initiation, related to Figure 5.
(A) Pearson correlation of KDM5A binding from this experiment with ENCODE data.
(B) ChIP-seq data at TP53 locus after depletion of KDM5A in HCT116 cells.
(**C**) Western blot for assessment of p53 after depletion of KDM5A and eIF4A2 in HCT116 cells.
(**D**) HCT116 cell lysate was immunoprecipitated with EIF4A2 antibody in RNA-immunoprecipitation buffer as shown in the top panel. The eluted RNA from the RNA-protein complexes was subject to reverse-transcription and PCR with *TP53* specific primers as shown in bottom panel.

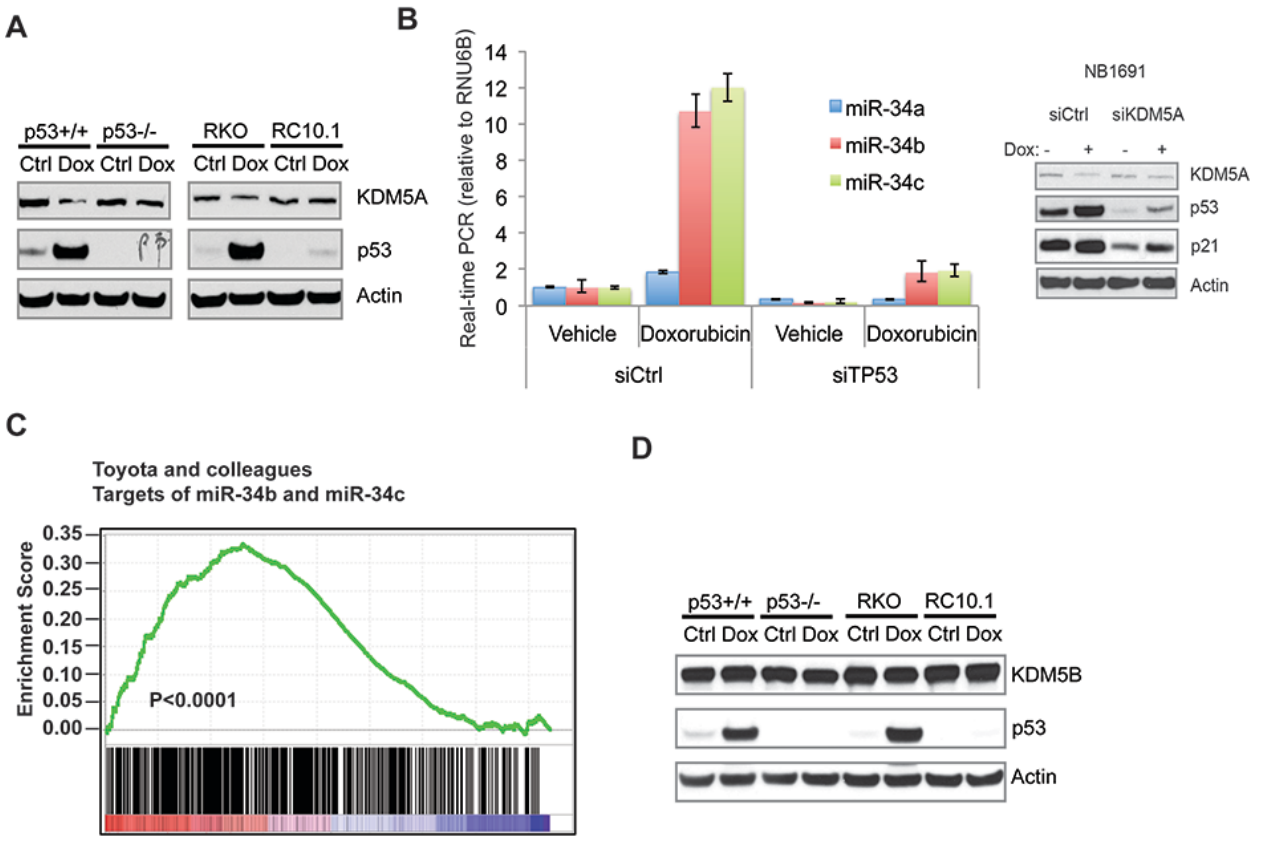

Figure S4. miR-34 targets KDM5A, related to Figure 7.

(A) p53+/+ and p53-/- HCT116, RKO and RC10.1 cells were treated with 0.2 μg/ml of doxorubicin for 48h and analyzed by western blot.

(**B**) NB-1691 cells transfected with p53 siRNA. 24h later, 0.2 μg/ml of doxorubicin was added for 48h treatment. Small RNA was extracted and analyzed by RT PCR for expression of miR-34s. The whole cell lysates were used for western blot (left panel)

(**C**) GSEA of miR-34b and miR-34c target gene set with transcriptional profiles of KDM5A knockdown in NB-1691 cells.

(**D**) p53+/+ and p53-/- HCT116, RKO and RC10.1 cells were treated with 0.2 μg/ml of doxorubicin for 48h and analyzed by western blot.

	Amp		Frequency of amplification				Del		Frequency of deletion		
	In Peak	Q-value	Overall	Focal	High-Level		In Peak	Q-value	Overall	Focal	High-Level
JMJD6	No	0.0000	0.2562	0.0632	0.0211	JMJD6	No	1.0000	0.1120	0.0163	0.0006
KDM1A	No	1.0000	0.0961	0.0221	0.0036	KDM1A	No	0.0000	0.2624	0.0996	0.0015
KDM1B	No	0.0000	0.2075	0.0359	0.0276	KDM1B	No	1.0000	0.1307	0.0144	0.0007
KDM2A	Yes	0.0000	0.1726	0.0729	0.0221	KDM2A	No	1.0000	0.1358	0.0119	0.0003
KDM2B	No	1.0000	0.1748	0.0280	0.0103	KDM2B	No	0.0171	0.1353	0.0325	0.0005
KDM3A	No	1.0000	0.1732	0.0252	0.0068	KDM3A	No	1.0000	0.0717	0.0126	0.0001
KDM3B	No	1.0000	0.1373	0.0231	0.0097	KDM3B	No	1.0000	0.2294	0.0157	0.0008
KDM4A	No	0.0000	0.1420	0.0427	0.0113	KDM4A	No	1.0000	0.1800	0.0174	0.0009
KDM4B	No	1.0000	0.1375	0.0200	0.0083	KDM4B	No	0.0000	0.2391	0.0714	0.0019
KDM4C	No	1.0000	0.1247	0.0287	0.0172	KDM4C	No	0.0000	0.3217	0.0279	0.0067
KDM4D	No	1.0000	0.1238	0.0260	0.0108	KDM4D	No	1.0000	0.2197	0.0168	0.0029
KDM5A	Yes	0.0000	0.2490	0.0570	0.0491	KDM5A	No	1.0000	0.1075	0.0205	0.0015
KDM5B	No	1.0000	0.3530	0.0302	0.0573	KDM5B	No	1.0000	0.0575	0.0098	0.0002
KDM5C	No	1.0000	0.1327	0.0222	0.0086	KDM5C	No	1.0000	0.1885	0.0088	0.0006
KDM6A	No	1.0000	0.1254	0.0182	0.0090	KDM6A	No	0.3560	0.2084	0.0182	0.0049
KDM6B	No	1.0000	0.0788	0.0085	0.0031	KDM6B	No	0.1110	0.3786	0.0247	0.0032
KDM8	No	1.0000	0.2037	0.0192	0.0172	KDM8	No	1.0000	0.1318	0.0068	0.0005
PHF2	No	1.0000	0.1192	0.0115	0.0065	PHF2	No	1.0000	0.2458	0.0136	0.0008
PHF8	No	1.0000	0.1394	0.0260	0.0102	PHF8	No	1.0000	0.1858	0.0075	0.0001

Table S1. The amplification (left) and deletion (right) of histone demethylases across 10844 tumors, related to Figure 1.

			Frequency of amplification		
Cancer subset	**In a Peak**	**Q value**	**Overall**	**Focal**	**High-level**
All cancers	Yes	1.91E-33	0.249	0.0547	0.0491
Epithelial cancers	Yes	6.58E-28	0.2742	0.0575	0.0546
Ovarian serous cystadenocarcinoma	Yes	2.04E-07	0.5699	0.2124	0.1779
Colon adenocarcinoma	Yes	3.50E-06	0.2422	0.0511	0.02
Breast invasive adenocarcinoma	Yes	1.07E-04	0.2611	0.0806	0.0463
Head and neck squamous cell carcinoma	Yes	2.54E-04	0.3199	0.0632	0.0575
Lung cancers	Yes	1.03E-03	0.3953	0.0816	0.061
Pancreatic adenocarcinoma	Yes	4.85E-03	0.212	0.0435	0.0272
Lung squamous cell carcinoma	Yes	2.03E-02	0.511	0.1038	0.0898
Rectum adenocarcinoma	Yes	2.78E-02	0.2424	0.0485	0.0485
Lung adenocarcinoma	Yes	7.22E-02	0.2829	0.0601	0.0329
Esophageal carcinoma	Yes	9.35E-02	0.3696	0.1033	0.0652
Uterine corpus endometrioid carcinoma	Yes	1.36E-01	0.1633	0.0455	0.026
Testicular germ cell tumors	Yes	2.18E-01	0.9667	0.06	0.68
Uveal melanoma	Yes	1.00E+00	0.0375	0	0
Colorectal cancers	No	5.92E-08	0.2423	0.0504	0.0276
Brain lower grade glioma	No	2.20E-07	0.1228	0.0585	0.0214
Glial cancers	No	2.89E-05	0.122	0.0404	0.022
Sarcoma	No	3.40E-01	0.2109	0.0938	0.043

Table S2. KDM5A amplification in all and independent cancers, related to Figure 1.

Table S3. Genetic data (amplification, deletion and mutation) of KDM5A, MDM2, TP53 from Xena UCSC dataset, related to Figure 1.

Table S4. KDM5A peaks for ChIP-seq analysis of KDM5A genomic binding in HCT116 cells, related to Figure 5.

Table S5. Genes encoding translational factors bound by KDM5A, related to Figure 5.

Table S6. H3K4me3 peaks for ChIP-seq analysis of H3K4me3 genomic enrichment in HCT116 cells after KDM5A knockout, related to Figure 5

Table S7. Connectivity map analysis of siRNA knockdwon of KDM5A in both p53+/+ and p53-/- HCT116 cells, related to Figure 5.

Score	Name
99.55	Protein Synthesis Inhibitor
98.39	ATPase Inhibitor
94.69	Tubulin Inhibitor
92.81	Proteasome Inhibitor
89.56	RNA Polymerase Enzymes
85.58	Proteasome Pathway
78.77	NFKB Activation
71.7	Ribosomal 40s Subunit
71.19	BMP Signaling
60.38	PKC Activator
46.83	DNA Replication
38.83	Cell Cycle Inhibition
37.52	NFKB Pathway Inhibitor
26.22	PKA Inhibitor
13.08	Nucleoporin
11.22	FXR Antagonist
3.48	IL4 Pathway
0.9	Vesicular Transport
0.9	AHSP Pathway
0.59	Ribonucleotide Reductase Inhibitor
0.2	Beta-Adrenergic Receptor Agonist
0.03	MTOR Inhibitor
0.02	Akt Signaling
-0.01	Non Homologous End Joining
-0.02	G2 M Checkpoint
-0.08	MEK Inhibitor
-0.14	Cyclooxygenase Inhibitor
-0.23	VEGFR Inhibitor
-0.35	PARP Inhibitor
-1.27	HDAC Inhibitor
-2.07	PI3K Signaling
-5.29	JAK Inhibitor
-6.43	HMGCR Inhibitor
-6.8	PI3K Inhibitor
-8.18	Serotonin Receptor Antagonist
-15.6	PKC Inhibitor
-28.59	Tachykinin Antagonist
-31.58	EIF Proteins
-69.12	GPCR Subset
-71.77	EGFR Inhibitor
-86.82	Src Inhibitor

TRANSPARENT METHODS

Cell culture

Isogenic $p53^{+/+}$ and $p53^{-/-}$ cell lines HCT116 (Bert Vogelstein, Baltimore, MD), RKO and RC10.1 (Michael Kastan, Durham, NC), A594, H1299, U2OS, SAOS2 (ATCC) cells were maintained in DMEM medium, supplemented with 10% FCS (HyClone, Thermo), 1% L-glutamine (MediaTech), 1% penicillin–streptomycin (Lonza), at 37 °C in 5% CO_2. IMR32, BE2(C), SK-N-SH and NB-1691 cells were maintained in RPMI medium supplemented with 10% FCS (HyClone, Thermo), 1% L-glutamine (MediaTech), 1% penicillin–streptomycin (Lonza). Cell lines were characterized by Short Tandem Repeat (STR) analysis by using Promega PowerPlex 16 HS System.

Identification of KDMs modulating p53 activity using focused siRNA library

After 24-hour plating of 2 X 10^5 of isogenic p53+/+ and p53-/- HCT116 cells in a 6-well plate, the p21-luciferease reporter (0-Luc, Addgene, plasmid#21723)(Zeng et al., 1997b) with the pRL *Renilla* luciferase control reporter vector (Promega) were transfected using Lipofectamine LTX reagent (Invitrogen). 24-hour later after reporter transfection, the siRNAs (Dharmacon) were reverse transfected using RNAiMax and plated into 96-well plate to a final concentration of 25 nM. After 72-hour siRNA transfection, dual-luciferase reporter assay was performed according to the instruction of manufacturer (Promega). The luciferase reading was done with BioTek. The p21-luciferase was normalized by renilla luciferase, which was then normalized with the non-targeting control 1 (NT1). Then the value for each gene was normalized with the value in $p53^{-/-}$ HCT16 cells. We picked up the genes as candidates with 2-fold induction as the threshold.

Transfection of miRNA and siRNA oligos

The Pre-miR™ miRNA Precursor molecules (hsa-miR-34a, hsa-miR-34b, hsa-miR-34c, and the control) are small, chemically modified double-stranded RNA molecules designed to mimic endogenous mature miRNAs, and were purchased from Ambion. The anti-miR-34s were purchased from Ambion. siRNA oligos for knockdown of p53, KDM5A, EIF2B4, and firefly luciferase control or Dharmacon Non-targeting control were synthesized by Dharmacon, Thermo Scientific. miRNAs or siRNAs were reversely transfected using RNAiMAX (Invitrogen) for 72-hour according to the manufacture's protocol. siKDM5A#1: UGACAAUGGUGGACCGCAU siKDM5A#4: GGAAAUACCCAGAGAAUGA, siTP53:GCAUCUUAUCCGAGUGGAA, siEIF2B4#1: GAGAUGUGAUCCUGGUAUA, siEIF2B4#3: AGCAGGUGAUUCAGGAUUA.

shRNA transduction

The TRC lentiviral-based shRNA knockdown plasmids for KDM5A were purchased from Open Biosystems, Thermo Scientific. TRCN0000014629 (5-TAAGTGTCCCTGTAAGTCTGG-3) had the best knockdown efficiency, and so was used in the in vivo experiments. The lentiviral shKDM5A and shControl (pLKO.1) particles were packaged by Vector Lab at St Jude. Briefly, HEK293T cells were transfected with shRNA constructs and helper plasmids (pCAG-kGP1-1R, pCAG4-RTR2, and pHDM-G). The 48- and 72-hr post-transfection replication-incompetent lentiviral particles were harvested and transduced into cells with 8μg/ml of polybrene. 48 hours later, 1 μg/ml of puromycin was added for selection for additional 48 hours before injection into mice or immunoblotting.

CRISPR/Cas9

The CRISPR/Cas9 system was used to truncate the *KDM5A* locus by targeting exons within the catalytic JmjC domain or PHD domain. After extensive bioinformatics analysis of the *KDM5A* locus integrated with data from ChIP-seq of histone marks, PAM sequences and off-target

algorithm, we designed 2 different sgRNAs. The sgRNA sequences targeting exon 11: tctctggtatgaaagtgccg, which targets the JmjC domain of KDM5A; exon16 sgRNA: acgactgacccaagtgtcat, which targets the region between JmjC and the second PHD domains. The paired DNA oligonucleotides containing sgRNA sequences were annealed and cloned into a PX458 (SpCas9-2A-EGFP-U6-sgRNA, Addgene 48138) all-in-one backbone. Clones were verified by Sanger sequencing using the U6 promoter forward primer 5'-gagggcctatttcccatgat-3'. All correct constructs were transfected into p53+/+ HCT116 cells and sorted for GFP. Single cell derived clones were validated for bi-allelic mutations via western blotting.

Immunoprecipitation

After 48h knockdown of KDM5A, HCT116 cells were lysed in immunoprecipitation buffer (25 mM Tris-HCl, pH7.5, 150 mM NaCl, 1 μM EDTA, 5% Glycerol, 1% NP40) with complete protease inhibitors (Roche) and phosphatase inhibitors (Roche) on ice. The pre-cleared lysates were incubated with 2 μg of mouse IgG (Cell Signaling), anti-p53 antibody (DO-1, Santa Cruz Biotechnology) and incubated with rotation at 4ºC overnight. 25 μl of protein A/G magnetic beads (Invitrogen) were added into each reaction for an additional 2-hour incubation. After the resin was washed 4 times with IP buffer, protein complexes were eluted with 60 μl of 2X SDS-PAGE sample buffer and subjected to SDS-PAGE and immunoblotting.

Western blot

Cell lysates were either prepared using RIPA buffer (Cell Signaling) supplemented with protease inhibitors (Roche complete mini), followed by 5 min heating at 75°C after addition of 2XSample Loading buffer (100 mM Tris-HCl pH 6.8, 4% SDS, 20% Glycerol, 5% β-mercaptoethanol, 0.2% Bromophenol blue). Alternatively, cells were directly lysed in 2XSample Loading buffer followed by 20 min heating at 95°C. Samples were separated on 4-12% Tris-glycine SDS-PAGE gels (Invitrogen), and transferred to PVDF membrane (Millipore). Membranes were blocked for 1hr in TBS buffer with 5% milk and 0.1% Tween 20, followed by overnight incubation with primary antibodies at 4°C. Membranes were washed for 3 x 5min at room temperature in TBS-T buffer. Mouse and rabbit HRP-conjugated secondary antibodies (ThermoFisher, 1:5,000) were incubated for 1 hr at room temperature followed by washing 3 x 5 min at room temperature in TBS-T. For detection, membranes were exposed to Pierce ECL Western Blotting Substrate and detected on Hyblot CL film (Denville Scientific Inc). All the western blot antibodies are listed: Rabbit anti-KDM5A Antibody, (Bethyl Laboratories, Inc.Cat# A300-897A, RRID:AB_2234038), Mouse Anti-p53 Monoclonal antibody, Clone DO-1 (Santa Cruz Biotechnology, Cat# sc-126, RRID:AB_628082), Mouse Anti-beta-Actin Monoclonal Antibody, Clone AC-15 (Sigma-Aldrich, Cat# A5441, RRID:AB_476744), p21 Waf1/Cip1 (12D1) (Cell Signaling Technology,Cat# 2947S, RRID:AB_823586), Mouse Anti-TIGAR Monoclonal Antibody, Clone M-209 (Santa Cruz Biotechnology, sc-166290, RRID:AB_2066582), MDM2 (SMP14) antibody (Santa Cruz Biotechnology, sc-965, RRID:AB_627920), PUMAα Antibody (B-6) (Santa Cruz Biotechnology, sc-377015), alpha Tubulin (B-7) antibody (Santa Cruz Biotechnology, sc-5286,RRID: AB_628411), Phospho-p53 (Ser15) Antibody (Cell Signaling Technology, Cat# 9284, RRID:AB_331464), 4E-BP1 (53H11) Rabbit mAb antibody (Cell Signaling Technology, Cat# 9644P, RRID:AB_10830220), eIF2B delta/EIF2B4 Antibody (Bethyl Laboratories, Cat# A302-982A, RRID:AB_10755230), eIF4AII (H-5) antibody (Santa Cruz Biotechnology, Cat# sc-137148, RRID:AB_2097384), V5 antibody Invitrogen (Cat# ABIN460705, RRID:AB_10804584), Anti-trimethyl-Histone H3 (Lys4) Antibody (EMD Millipore, Cat# 07-473, RRID:AB_1977252), Anti-biotin (Bethyl Labs, A150-109A, RRID:AB_67327), Anti-GAPDH (Cell Signaling Technologies, 5174S, RRID:AB_10622025), Anti-H3K4me3 (Millipore 07-473, RRID:AB_1977252).

RT-PCR

RNA was recovered using RNeasy Mini Kit from Qiagen and cDNA was synthesized using SuperScript III First-Strand Synthesis System (Invitrogen). RT-PCR was performed using Applied Biosystems 7500 Real-Time PCR system. The results were analyzed using delta delta Ct methods. PCR primers are listed: ACTIN Forward: CCAACCGCGAGAAGATGA, ACTIN Reverse: CCAGAGGCGTACAGGGATAG; CDKN1A Forward: CCGAAGTCAGTTCCTTGTGG, CDKN1A Reverse: CATGGGTTCTGACGGACAT; KDM5A Forward: TGGATTTCCGGTGAAGGAT, KDM5A Reverse: TCCAGGACAGGCATGTTATTC; TP53 Forward: AGGCCTTGGAACTCAAGGAT, TP53 Reverse: CCCTTTTTGGACTTCAGGTG; GAPDH Forward: AACGGGAAGCTTGTCATCAATGGAAA, GAPDH Reverse: GCATCAGCAGAGGGGGCAGAG; 18S Forward: GCTTAATTTGACTCAACACGGGA; 18S Reverse: AGCTATCAATCTGTCAATCCTGTC.

Overexpression of KDM5A

HCT116 cells were transfected with either pcDNA6.2 N-emGFP Dest (empty vector) or pcDNA6.2 N-emGFP-KDM5A(Gong et al., 2017) using Lipofectamine 3000 reagent (Thermo). Following transfection, GFP-positive cells were sterile sorted using flow cytometry and harvested for western blot analysis.

Affymetrix microarray analysis

RNA was extracted using RNeasy Mini Kit from Qiagen 72-hour after transfection with two different siRNA oligos (siKDM5A#1, siKDM5A#4). siRNA controls were purchased from Dharmacon. After quality control with Agilent RNA analyzer, RNA was subjected to hybridization using an Affymetrix HT HG-U133+ PM 16-Array Plate (for NB-1691 and SK-N-BE2) or HuGene_2.0_st chip for isogenic $p53^{+/+}$ and $p53^{-/-}$ HCT116 cells. The KDM5A knockdown samples were compared with the controls using Gene Set Enrichment Analysis (GSEA). Differential gene expression was analyzed by t-test using the Differential Expression Analysis module at GenePattern server (http://genepattern.broadinstitute.org/gp/pages/protocols/DiffExp.html).

Molecular concept analysis

For molecular concept analysis, the genes upregulated by KDM5A depletion in p53+/+ HCT116 cells were upload into the Oncomine program (www.oncomine.com) and concept analysis was performed. Here we focused on the "molecular subtype mutation" concepts association with KDM5A targets. The associated concepts with odds ratio <2, p value<0.001 were filtered out. The network of the associated concepts was displayed using Cytoscape program (http://cytoscape.org/).

TCGA and cBioportal data analysis for correlation of KDM5A amplification and TP53 mutation

To analyze the copy number alterations of histone demethylases we mined TCGA Tumorscape (http://www.broadinstitute.org/tcga/pages/portalHome.jsf), which is designed to facilitate the use of high-resolution copy number data amassed from multiple cancer types (all generated through TCGA) (Beroukhim et al., 2010). It enables downloading and interactive viewing of cancer copy-number profiles across several dozen cancer types, gene-level queries to determine the rate and significance of alteration of every gene, and cancer-type-level queries to identify the significant regions of copy-number alteration.

To investigate the mutual exclusivity of genetic alterations of TP53 and KDM5A, we used the UCSC Xena program (https://xenabrowser.net) to download the data that contained gene copy calculations from the cohort of TCGA Pan-Cancer (PANCAN). We downloaded the gene-level copy number (gistic2_thresholded) of *KDM5A*, *MDM2* and *TP53*. We then downloaded somatic

non-silent TP53 mutations (gene-level) from the dataset of "somatic gene-level non-silent mutation (ucsc) data" from the PANCAN cohort. After combining all data together, we had 2623 samples that consisted of calculated data for both KDM5A and TP53. To examine the relationship of KDM5A amplification and TP53 somatic mutation, we excluded samples that had TP53 deletion with both alleles, resulting in 2575 cases for analysis. We then calculated the frequency difference using contingency table for Fisher's exact test by using Prism software.
For Figure 1G and 1H, we employed genetic alteration data by using cBioportal program (http://www.cbioportal.org/). We combined 6 different types of cancers including low grade gloma (TCGA, provisional), lung squamous cell carcinoma (TCGA, provisional), ovarian cancer (TCGA, provisional), neuroendocrine prostate cancer (Trento/Cornell/Broad 2016), testicular germ cell cancer (TCGA, provisional), which had a higher incidence of KDM5A amplification (>5%) than other types of cancer.

Data mining
The expression of KDM5A from RNA-seq (GSE62564) was downloaded from R2 program and analyzed by one-way ANOVA using Prism software. A Kaplan-Meier survival curve was generated using R2 program (http://r2.amc.nl). The median value of KDM5A expression was used for the cut-off level of KDM5A expression in survival analysis. For connectivity map analysis, the common genes upregulated and downregulated by KDM5A knockdown in both p53+/+ and p53-/- HCT116 cells were uploaded into program (https://clue.io/) for connectivity map analysis.

ChIP-seq
To detect the genomic enrichment of H3K4me3 and KDM5A, $2X10^7$ HCT116 cells (2 clones for CRISPR controls, 2 clones for CRISPR KDMA) were cross-linked for 5 min with 1% formaldehyde, quenched with 125 mM glycine for 5 min, washed in cold PBS, and resuspended in Cell Lysis Buffer (10 mM Tris-HCl pH 8.0, 10 mM NaCl, 0.2% NP40, and protease inhibitors). The nuclear pellet was resuspended with Nuclei Lysis Buffer (50 mM Tris-HCl pH 8.0, 10 mM EDTA, 1% SDS, and protease inhibitors). Chromatin fragments (100-300 bp) obtained by sonication (Covaris) were resuspended in 150 mM NaCl, 20 mM Tris-HCl pH 8.0, 2 mM EDTA, and 1% Triton X-100, 0.01% SDS then incubated for 4 hours at 4°C with magnetic beads (Dynal) conjugated to H3K4me3 (07-473, EMD Millipore) or KDM5A (A300-897, Bethyl Laboratory). Beads were washed, DNA was eluted, and cross-links were reversed in 1% SDS and 0.1 M NaHCO3 overnight at 65°C. DNA was purified using a PCR purification kit (Qiagen). Libraries were prepared from the ChIP material using the ChIP-Seq Sample Prep Kit (Illumina) and sequenced on Illumina HiSeq 2000 (50-bp reads).
BWA (version 0.5.9-r26-dev, default parameters) was used to align both input and sample ChIP-seq reads to the hg19 reference genome (GRCh37-lite). Duplicated reads were marked using Picard (version 1.65(1160)) (http://picard.sourceforge.net). Samtools (version: 0.1.17 (r973:277)) with the -q 1 -F 1024 parameters was used to exclude duplicated reads. For quality control (QC) purposes and to estimate fragment size, SPP (version 1.11, for samples with duplicates removed) was used to generate cross-correlation plots using R (version 2.14.0) with the caTools(version 1.17) and bitops (version 1.0-6) packages. All data passed QC following ENCODE criterion.
BAM files were converted to BED files using bamToBed (Bedtools version 2.17.0). The fragment sizes estimated by SPP were used to extend each read in a new BED file. Per base coverage was determined with genomeCoverageBed (Bedtools) and scaled to 15 million reads total. A bigwig file for viewing within the Integrative Genome Viewer (IGV) (version 2.3.57 (84)) was generated using bedGraphToBigWig (Bedtools). MACS2 (version 2.0.9 20111102, nomodel with extsize defined as fragment size estimated by SPP) was used to call peaks from the original BED file generated above. For each each different ChIP-Seq experiment

(H3K4me3, KDM5A), peaks were combined using merge from Bedtools. Reads from each sample were mapped to the merged peaks using bedmap (Bedops version 2.4.2) to get a count of the number of reads per sample for each peak.

ENOCDE data analysis

The bigwig files of ChIP-seq data, KDM5A (accession number ENCFF000AYU) from human H1 embryonic stem cells were downloaded from ENCODE (https://www.encodeproject.org/search/?type=experiment). The signals of the binding on the specific genomic loci were visualized using IGV_2.3.53 program downloaded from http://www.broadinstitute.org/software/igv/node/250.

Pulse-Chase Assay with [^{35}S]Methionine and [^{35}S]Cysteine labeling

HCT116 ($p53^{+/+}$) cells were transfected with siKDM5A. 48 hours after transfection, cells were starved in cysteine- and methionine-free modified Eagle's medium (MEM) supplemented with 10% dialyzed FBS for 30 min and then radiolabeled with 75 µCi of [^{35}S]methionine and [^{35}S]cysteine (PerkinElmer Life Sciences) for 30 min. The radiolabel in the cells was then chased in full DMEM supplemented with 10% FBS, 3 mM methionine and 3 mM cysteine at 37 °C. When used, 5 µM MG132 was added to the pulse labeling medium to prevent protein degradation and maintained during the chase part of the experiment. At the appropriate chase time, cells were harvested on ice by washing 2 times with cold PBS and lysed in radioimmune precipitation assay buffer (25 mM Tris-HCl (pH 7.4), 150 mM NaCl, 1% Nonidet P-40, 1% sodium deoxycholate, 0.1% SDS) supplemented with protease inhibitors (Roche). The clear lysates were collected after centrifugation at 4 °C for 10 min at 13,000 × *g*. p53 protein was then immunoprecipitated using p53 antibody (DO-1, Santa Cruz) from the supernatant and resolved on SDS PAGE.

Polysome profiling

Cells were plated at 5 million cells per 150mm dish in DMEM supplemented with 10% FBS. Once cells reached 80% confluency, they were incubated with growth media containing 100ug/mL (final concentration) of cycloheximide (CHX) for 5 minutes at 37^{o}C and 5% CO_2. Following, cells were washed twice with ice-cold PBS containing 100ug/mL (CHX) and harvested in 5mL of ice-cold PBS +100ug/mL CHX by scraping into a 50mL conical tube. Cells were centrifuged at 200xg for 5 minutes at 4^{o}C, and the cell pellet was resuspended in hypotonic lysis buffer (5mM Tris-HCl (pH 7.5), 1.5mM KCl, 2.5mM $MgCl_2$, 1% Triton X-100, 1% deoxycholate, 100ug/mL CHX, 1mM dithiothreitol, 200U/mL RNase inhibitor (New England Biolabs #M0314L), and EDTA-free cocktail protease inhibitor (Roche)). Cells were centrifuged at 16,000xg for 7 minutes at 4oC, and the supernatant (lysate) transferred to a new, pre-chilled tube. 10% of the lysates were isolated as input samples for cytosolic steady-state mRNA levels where they were flash-frozen in Trizol (Ambion) in liquid nitrogen and stored at -80^{o}C. 500uL of each lysate was carefully layered onto linear sucrose gradients (5-50% sucrose in 200mM HEPES, 1M KCl, 50mM $MgCl_2$, 100ug/mL CHX, EDTA-free cocktail protease inhibitor (Roche), and 100 U/mL RNase inhibitor) which were prepared in 14 x 8mm Ultra-Clear centrifuge tubes (Beckman Coulter 344059). Lysate-loaded gradients were ultra-centrifuged at 36,000rpm for 2 hours at 4^{o}C. Following centrifugation, 500uL fractions were collected by hand by piercing the bottom of each tube with a 19G needle. The absorbance at 260nm was measured for each fraction and input, and flash frozen in Trizol reagent in liquid nitrogen and store at -80^{o}C. RNA was extracted following the manufacturer's protocol, and an equal quantity of RNA from each fraction was converted into cDNA using the SuperScript IV kit (ThermoFisher), and then analyzed by qRT-PCR.

Click-iT Labeling Assay for Metabolic Labeling of Newly Synthesized Proteins
Cells were plated at 5 million cells per 100mm dish in DMEM supplemented with 10% FBS. Cells were washed with warm PBS and replaced with methionine-free medium (Thermo 21013024 supplement with glutamine and sodium pyruvate) for 1 hour at 37°C 5% CO_2. Following, fresh methionine-free media containing 50uM of Click-iT AHA (L-azidohomoalanine) (Thermo C10102) was added to the cells for 2 hours at 37°C. After AHA-labeling, cells were washed with warm PBS and lysed with 1% SDS, 50mM Tris-HCl, (pH 8.0) supplemented with phosphatase (PhosSTOP, Sigma) and protease (cOmplete mini, Roche) by applying the buffer directly to the plate, incubating the cells on ice for 30 minutes, tilting the plates, and collecting the lysate. Lysates were briefly sonicated, vortexed for 5 minutes, and centrifuged at 18,000xg for 5 minutes at 4°C. Total protein quantification was assayed using the EZQ Protein Quantification Kit (Thermo R33200) according to the manufacturer's protocol and results were read on a fluorescence-based microplate reader (BioTek Synergy 2). Click chemistry of the biotin-alkyne (PEG4 carboxamide-propargyl biotin) (Thermo B10185) to the AHA-labeled lysates was performed using the Click-iT Protein Reaction Buffer Kit (Thermo C10276) using a concentration of 40uM biotin-alkyne per click reaction (and no biotin-alkyne added for controls). Following the click reaction, samples were either assayed for total biotinylated protein by following the manufacturer's protocol or directly continued after the click reaction for immunoprecipitation. For total biotinylated protein, briefly, 600uL of methanol, 150uL of chloroform, and 400uL of megaOhm water was sequentially added and vortexed, followed by centrifugation at 18,000xg for 5 minutes. The upper aqueous phase was discarded, and 450uL of methanol was added, vortexed, and centrifuged again at 18,000xg for 5 minutes. This methanol step was performed in duplicate to remove residual reaction components. Protein pellets were allowed to air dry and resuspended in a suitable volume of sample buffer and heated prior to western blot analysis. For immunoprecipitation, 2ug of anti-p53 antibody (DO-1; Santa Cruz; sc126) was bound to 10uL of magnetic beads per sample (Dynabeads M280 Sheep anti-mouse IgG (Invitrogen, 11201D)) for 1 hour in PBS. Beads were subsequently washed and added directly to the click reaction step along with 800uL of RIPA buffer (Thermo 89900) and left to rotate end-over-end at 4°C overnight. The following day, beads were washed 3 times with RIPA buffer and eluted with sample buffer at 95°C for 25 minutes.

RNA-immunoprecipitation
RNA immunoprecipitation was performed as previously described (Rinn et al., 2007). Briefly, 2.5 ug V5 antibody (Invitrogen) or control mouse IgG and 20ul of Protein A/G plus beads (Thermo Scientific) were incubated with 2mg of p53+/+ HCT116 cell lysate transfected with eIF4A2 plasmid, and incubated for 3 hrs at 4°C with gentle rotation. The beads were then washed five times with RIP buffer, and the RNAs were extracted with Trizol reagent (Invitrogen), followed by standard RNA precipitation protocols. The RNA was resuspended in 30 µl of RNase-free water and subjected for PCR analysis. A fraction of immunoprecipitated protein were used for western blotting to confirm the immunoprecipitation.

Luciferase reporter assay
After 24 hour siRNA knockdown of KDM5A in p53++ and p53-/- HCT116 cells by reverse transfection in 6-well plate, 2.4 µg after 24 hour siRNA knluciferease reporter plasmid (145-pGL3ctrl-3' UTR, addgene# 28175) (Chen and Kastan, 2010) and 0.1 µg anpRL *Renilla* Luciferase Control Reporter Vector (Promega) were transfected by Lipofectamine™ 3000 Transfection Reagent (Invitrogen). 48 hours later, cells were harvested for the dual luciferase assay according to the instructions of manufacturer (Promega).

Animal experiments
All murine experiments were done in accordance with a protocol approved by the Institutional Animal Care and Use Committee of St. Jude Children's Research Hospital. Lentivirus was used to transduce isogenic $p53^{+/+}$ and $p53^{-/-}$ HCT116, SK-N-SH, BE2(C) and NB-1691 cells for shRNA knockdown of KDM5A. After transduction, 1 μg/ml of puromycin was used for selection of stable knockdown. Subcutaneous xenografts were established in male CB-17 severe combined immunodeficient mice (Taconic, Hudson, NY). Tumors measurements were performed weekly using handheld calipers, and volumes calculated as width π/6 xd3 where d is the mean of two diameters taken at right angles.

Statistical Analysis
For Figure 1b and 1c, the mutual exclusivity of pairs of mutations was evaluated with the use of two-by-two contingency tables and Chi-square test. A p value of less than 0.05 was considered statistically significant. Analyses were conducted in R-3.2.5. Each experiment was carried out at least in triplicate. To determine statistical significance, the unpaired, two-tailed Student's *t* test was calculated using the *t* test calculator available on GraphPad Prism 7.0 software. Fisher's exact test was performed for frequency distribution in contingency table. A p value of less than 0.05 was considered statistically significant. Tumor growth statistical comparisons were performed by ANOVA using PRISM program.

Data and Software Availability

All microarray and deep sequencing data have been deposited in GEO under accession number: GSE45967, GSE49854, GSE100511, GSE107221.

SUPPLEMENTAL REFERENCES
Chen, J., and Kastan, M.B. (2010). 5'-3'-UTR interactions regulate p53 mRNA translation and provide a target for modulating p53 induction after DNA damage. Genes Dev *24*, 2146-2156.

Rinn, J.L., Kertesz, M., Wang, J.K., Squazzo, S.L., Xu, X., Brugmann, S.A., Goodnough, L.H., Helms, J.A., Farnham, P.J., Segal, E.*, et al.* (2007). Functional demarcation of active and silent chromatin domains in human HOX loci by noncoding RNAs. Cell *129*, 1311-1323.

Zeng, Y.X., Somasundaram, K., and el-Deiry, W.S. (1997a). AP2 inhibits cancer cell growth and activates p21WAF1/CIP1 expression. Nat Genet *15*, 78-82.